

Epigenetic and Oncogenic Inhibitors Cooperatively Drive Differentiation and Kill KRAS-Mutant Colorectal Cancers



Patrick Loi^{1,2}, Amy E. Schade^{1,2}, Carrie L. Rodriguez^{1,2}, Anjana Krishnan^{1,2}, Naiara Perurena^{1,2}, Van T.M. Nguyen³, Yilin Xu^{4,5,6,7}, Marina Watanabe^{1,2}, Rachel A. Davis^{1,2}, Alycia Gardner^{1,2}, Natalie F. Pilla^{1,2}, Kaia Mattioli^{1,2}, Olesja Popow^{2,8}, Nuray Gunduz^{9,10}, Tamsin R.M. Lannagan^{9,10}, Samantha Fitzgerald^{2,8,11}, Ewa T. Sicinska⁸, Jia-Ren Lin^{4,5,6,7}, William Tan⁸, Lauren K. Brais⁸, Kevin M. Haigis^{2,8}, Marios Giannakis^{2,8,11}, Kimmie Ng⁸, Sandro Santagata^{4,5,6,7}, Kristian Helin³, Owen J. Sansom^{9,10}, and Karen Cichowski^{1,2,4}

ABSTRACT

Current treatments for *KRAS*-mutant colorectal cancers are often limited by cellular plasticity and rewiring responses. Here we describe a promising therapeutic strategy that simultaneously targets epigenetic and oncogenic signals. Specifically, we show that inhibitors of histone methyltransferase, EZH2, synergize with various rat sarcoma virus (RAS) pathway inhibitors and promote dramatic tumor regression *in vivo*. Together these agents cooperatively suppress Wingless and Int-1 (WNT)-driven transcription and drive colorectal cancers into a more differentiated cell state by inducing the Groucho/transducin-like enhancer corepressor, *TLE4*, along with a network of WNT pathway inhibitors and intestinal differentiation proteins. However, these agents also induce the proapoptotic protein BCL2 modifying factor (BMF), which subsequently kills these more differentiated cells. Accordingly, cell death can be prevented by activating β -catenin, by blocking differentiation, or by ablating *BMF* expression. Collectively, these studies reveal a new therapeutic approach for treating *KRAS*-mutant colorectal cancers and illustrate a critical convergence of EZH2 and RAS on oncogenic WNT signals, intestinal differentiation, and apoptosis.

SIGNIFICANCE: Combined EZH2 and RAS pathway inhibitors kill *KRAS*-mutant colorectal cancer cells and promote durable tumor regression *in vivo*. These agents function by cooperatively suppressing the WNT pathway, driving differentiation, and epigenetically reprogramming cells to permit the induction of apoptotic signals, which then kill these more differentiated tumor cells.

INTRODUCTION

Colorectal cancers represent the second highest cause of cancer mortality worldwide, with a 5-year survival rate of <13% for advanced disease (1–3). Many colorectal cancers exhibit hyperactivated RAS/RAF/MEK/ERK signaling, with activating *KRAS* mutations occurring in 40% to 50% of all colorectal cancers (4–7). Conventional chemotherapies have limited efficacy in advanced tumors, and single-agent kinase inhibitors, including MEK- and EGFR-targeted therapies, are ineffective against colorectal cancers that harbor *KRAS* mutations (8, 9). Fortunately, the *KRAS*^{G12C} inhibitor, adagrasib, combined with the EGFR-directed antibody, cetuximab, has

demonstrated promising clinical activity, resulting in accelerated FDA approval for progressive *KRAS*^{G12C}-mutant tumors (10). Nevertheless, *KRAS*^{G12C} mutations are relatively infrequent in colorectal cancers, representing only 11% of *KRAS* mutations in these malignancies, and are only present in 3% of colorectal cancers overall (11). In addition, clinical responses to these agents are generally incomplete and not durable. Thus, there is a critical need for developing additional improved therapies for *KRAS*-mutant colorectal cancers.

Disease heterogeneity and cellular plasticity both hamper the efficacy of targeted therapies and contribute to *de novo* and acquired resistance in colorectal cancer (12). In intestinal cells, cellular plasticity is often regulated by epigenetic mechanisms, which allow cells to dynamically alter their differentiation state in response to injury, inflammation, and stress (13). During tumor development, nonmutational epigenetic reprogramming through the dysregulation of epigenetic regulators is also thought to control tumor cell plasticity (14). Therefore, we hypothesized that targeting a traditional oncogenic signal along with a critical epigenetic regulator might offer a powerful therapeutic approach if we were able to drive or lock cells into a more vulnerable cell state.

EZH2, the catalytic component of polycomb repressive complex 2 (PRC2), is a major epigenetic regulator and is commonly overexpressed in solid tumors (15). Polycomb group proteins are highly conserved developmental regulators that maintain cellular identity by dynamically silencing key genes involved in differentiation (16, 17). *EZH2* silences transcription at specific genomic sites by methylating histone 3 at lysine 27 (H3K27me3), thereby reducing chromatin accessibility to transcriptional machinery (15, 18). Notably, alterations in *EZH2* have been proposed to play an important role in many tumor types (19–21). Although activating mutations in *EZH2* have been detected in a subset of cancers, such as

¹Genetics Division, Department of Medicine, Brigham and Women's Hospital, Boston, Massachusetts. ²Harvard Medical School, Boston, Massachusetts. ³Division of Cancer Biology, The Institute of Cancer Research, London, United Kingdom. ⁴Ludwig Center at Harvard, Boston, Massachusetts. ⁵Laboratory of Systems Pharmacology, Harvard Medical School, Boston, Massachusetts. ⁶Department of Systems Biology, Harvard Medical School, Boston, Massachusetts. ⁷Department of Pathology, Brigham and Women's Hospital, Harvard Medical School, Boston, Massachusetts. ⁸Dana Farber Institute, Boston, Massachusetts. ⁹CRUK Beatson Institute, Glasgow, United Kingdom. ¹⁰School of Cancer Sciences, University of Glasgow, Glasgow, United Kingdom. ¹¹Broad Institute of MIT and Harvard, Cambridge, Massachusetts.

P. Loi and A.E. Schade contributed equally to this article.

Corresponding Author: Karen Cichowski, Harvard University, 77 Avenue Louis Pasteur, 458D NRB, Boston, MA 02115. E-mail: kcichowski@rics.bwh.harvard.edu

Cancer Discov 2024;14:2430–49

doi: 10.1158/2159-8290.CD-23-0866

This open access article is distributed under the Creative Commons Attribution-NonCommercial-NoDerivatives 4.0 International (CC BY-NC-ND 4.0) license.

©2024 The Authors; Published by the American Association for Cancer Research

lymphomas and melanomas, *EZH2* is more commonly overexpressed in solid tumors (22–25). PRC2 is known to play a broad role in stem cell maintenance and has been proposed to regulate the differentiation of intestinal cells (26); however, little is known about how *EZH2* overexpression contributes to the development or maintenance of colorectal cancers.

In this study, we show that combined *EZH2* and RAS pathway inhibitors potentially kill colorectal cancer cells and promote dramatic tumor regression in multiple models *in vivo*. We further show that these agents converge by upregulating genes that suppress the WNT pathway, drive intestinal differentiation, and trigger apoptosis, all of which contribute to this synergy. Together, these findings reveal a promising therapeutic strategy for advanced colorectal cancer, elucidate the mechanism by which these agents function, and illustrate a paradigm for developing epigenetic-based combination therapies.

RESULTS

EZH2 Inhibitors Sensitize KRAS-Mutant Colorectal Cancer to RAS Pathway Inhibitors

Analysis of the Cancer Genome Atlas (TCGA) Firehose Legacy dataset reveals that *EZH2* is overexpressed in >66% of all samples from patients with colorectal cancer when compared with normal tissue (Fig. 1A). Notably, *EZH2* is overexpressed in a similar percentage of *KRAS*-mutant tumors (61%), and equally high expression levels are observed in tumors that harbor different *KRAS*-mutant alleles (Supplementary Fig. S1A). To determine whether *EZH2* inhibition might sensitize colorectal cancers to RAS pathway inhibitors, we first evaluated these agents in a panel of human cell lines harboring a variety of *KRAS* mutations. Tumor cells were pretreated for 5 days with the *EZH2* inhibitor tazemetostat (EPZ-6438) to allow for the turnover and loss of H3K27me3 (27), followed by the addition of trametinib (Supplementary Fig. S1B). Because colorectal cancer cell lines exhibit different sensitivities to trametinib, a dose that exerted the maximal cytostatic response was empirically determined for each cell line (1–50 nmol/L; Supplementary Fig. S1C) and was used to facilitate comparison (Fig. 1B). *EZH2* inhibition alone exerted minimal or occasional cytostatic effects; however, when exposed to both agents, cells rapidly died, as demonstrated by a loss of 50% to 75% of cells after only 5 days of co-treatment (Fig. 1B). Moreover, whereas single concentrations of trametinib are shown in Fig. 1B, tazemetostat broadly enhanced the effects of trametinib at multiple doses (Supplementary Fig. S1C), and the effects were synergistic, as determined by the highest single agent (HSA) synergy model (Fig. 1C; Supplementary Fig. S1D).

In all cell lines, tazemetostat and trametinib effectively inhibited H3K27me3 and pERK, respectively, and a pattern of cooperative suppression of either target was not observed (Fig. 1D). *EZH2* was overexpressed in all of these tumor cell lines, and small differences in *EZH2* expression did not correlate with subtle differences in sensitivity to these agents (Supplementary Fig. S1E). Notably, the response to combined *EZH2* and MEK inhibition was durable, and cells continued to die for at least 2 weeks (Fig. 1E). Importantly, this drug

combination did not kill normal human intestinal epithelial cells (Supplementary Fig. S1F). Finally, to determine whether cells were dying via apoptosis, caspase-3/7 activity was measured using live-cell imaging. Whereas trametinib alone induced low levels of apoptosis, together these agents triggered cell death in 60% to 75% of cells in less than 40 hours (Fig. 1F; Supplementary Fig. S1G).

MEK inhibitors were used for the studies described above because the majority of *KRAS* mutations found in colorectal cancers are still not directly targetable by clinically approved agents. However, *KRAS*^{G12D} accounts for 33% of *KRAS* mutations in this tumor type (28). To determine if *EZH2* inhibition could also enhance the effects of recently developed *KRAS*^{G12D} inhibitors, cells were pretreated with tazemetostat and then exposed to increasing concentrations of MRTX1133 (29). Tazemetostat substantially sensitized colorectal cancers to this inhibitor (Fig. 1G). Notably, colorectal cancer cells harboring the *KRAS*^{G12C} allele also exhibited enhanced sensitivity to the covalent *KRAS*^{G12C} selective inhibitor, MRTX849, when combined with tazemetostat (Fig. 1H). These effects could be recapitulated using a different MEK inhibitor, binimetinib (Supplementary Fig. S1H), or by replacing the *EZH2* inhibitor with an embryonic ectoderm development (EED) inhibitor, which suppresses another obligate PRC2 component (Supplementary Fig. S1I).

To determine if these effects might extend to *BRAF*-mutant colorectal cancers and/or whether they were dependent on RAS pathway activation at all, additional colorectal cancer models were investigated. Four *BRAF*^{V600E} colorectal cancer cell lines were pretreated with tazemetostat and then exposed to either trametinib, the *BRAF*^{V600E} mutant-selective inhibitor encorafenib, or the recently approved combination of encorafenib plus cetuximab, which inhibits feedback activation of the RAS pathway (30). In all settings, tazemetostat potentiated the effects of these RAS pathway inhibitors (Fig. 1I), which was observed at multiple doses (Supplementary Fig. S1J). By contrast, *EZH2* inhibition did not trigger a cooperative cytotoxic response when combined with trametinib at any dose in three additional lines that lacked *KRAS* or *BRAF* mutations (Fig. 1J; Supplementary Fig. S1K). Taken together, these findings demonstrate that *EZH2* inhibition broadly enhances the cytostatic effects of RAS pathway inhibitors in colorectal cancers but only in tumors driven by mutations in RAS pathway components.

Combined Suppression of EZH2 and the RAS Pathway Promotes Tumor Regression in Multiple In Vivo Models and Enhances Survival

To evaluate the efficacy of this therapeutic strategy *in vivo*, a cell-derived xenograft (CDX) model (LOVO) and four patient-derived xenograft (PDX) models were generated (COCA74P, derived from a primary rectal tumor with a *KRAS*^{G12V} mutation; COCA9, derived from a previously treated liver metastasis with a *KRAS*^{G12V} mutation; COCA4, derived from a primary tumor with a *KRAS*^{G12D} mutation from an individual with Lynch syndrome; and COCA30, derived from a previously treated primary tumor with a *KRAS*^{G12D} mutation; refs. 31, 32). Similar to the design of *in vitro* studies, mice with established tumors were pretreated with the *EZH2* inhibitor or vehicle for 7 days before the addition of trametinib,

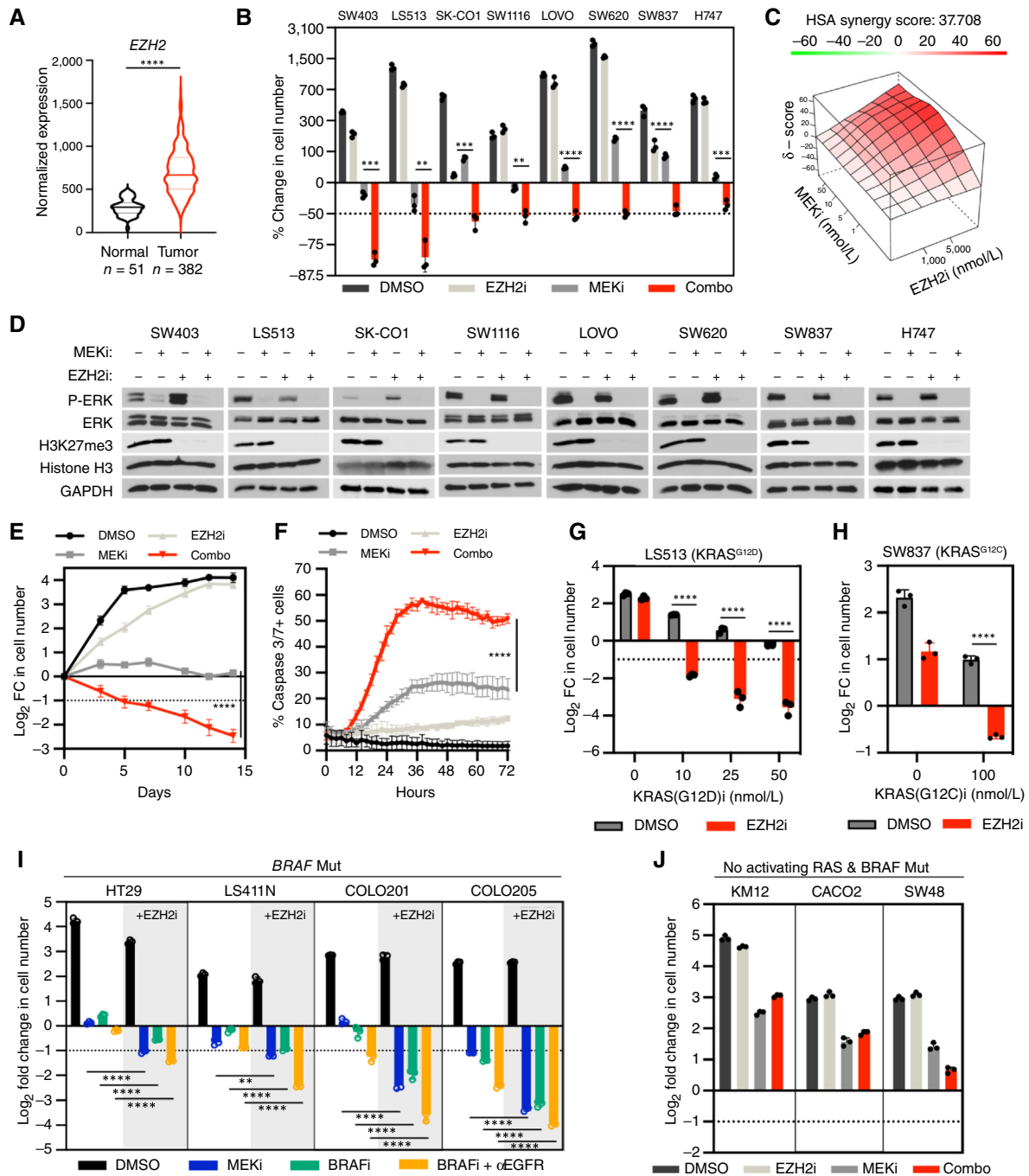


Figure 1. EZH2 inhibitors dramatically sensitize KRAS-mutant colorectal cancer to RAS pathway inhibitors. **A**, EZH2 mRNA levels in colorectal cancer tumors and matched normal colonic tissue. Sixty-six percent of colorectal cancer tumors have EZH2 expression two-fold higher (78.5% have two standard deviations higher) than the mean of normal colonic tissue. **B**, Proliferation assay over 5 days in a panel of KRAS-mutant colorectal cancer cell lines treated with DMSO, EZH2 inhibitor (5 μmol/L tazemetostat), MEK inhibitor (1–50 nmol/L trametinib, see “Methods”), or combination. Graph reflects the relative change in cell number (log₂ fold scale to best visualize loss of cells) compared with day 0. **C**, Synergy plots depicting Gaddum’s non-interaction model (HSA) for LOVO cells treated with EZH2i and/or MEKi. **D**, Immunoblots depicting relative levels of MEK target inhibition (pERK) and EZH2 target inhibition (H3K27me3) and relevant loading controls after 16–24 hours of treatment with indicated compounds in cell lines from **B**. **E**, Proliferation assay of LOVO cells treated with EZH2i or MEKi over 14 days. Unpaired two-tailed t test between MEKi- and combo-treated cells at last timepoint. **F**, Percentage caspase 3/7+ (apoptotic) LOVO cells after treatment with the indicated agents over time measured by Incucyte live-cell imaging. *P* value determined by ANOVA. **G** and **H**, Proliferation assay in several cell lines harboring KRAS^{G12D} or KRAS^{G12C} mutations after treatment with the indicated compounds (MRTX1133—KRAS^{G12D} inhibitor in **G** or MRTX849—KRAS^{G12C} inhibitor in **H**). **I**, Proliferation assay of a panel of BRAF^{V600E}-mutant colorectal cancer cell lines over 5 days treated with MEKi (trametinib), BRAFi (encorafenib), αEGFR (cetuximab), and/or EZH2i (tazemetostat). Concentrations are reported in “Methods” for each cell line. **J**, Proliferation assay in a panel of colorectal cancer cell lines with no activating mutations in KRAS or BRAF over 5 days, treated with EZH2i (tazemetostat) and/or MEKi (trametinib). Unless otherwise indicated, for all subfigures bars represent mean ± SD. *P* value measured by unpaired t test. *, *P* < 0.05; **, *P* < 0.01; ***, *P* < 0.001; ****, *P* < 0.0001. A loss of 50% of cells or a log₂ fold change of –1 is denoted with a dotted line.

Downloaded from <http://aacrjournals.org/cancerdiscovery/article-pdf/14/1/224/30351937/1.cd-23-0866.pdf> by guest on 29 April 2025

and treatment continued for a total of 28 days. Notably, EZH2 or MEK inhibition alone had minimal effects on tumor growth throughout the entire duration of treatment in all three models (Fig. 2A–J). However, combined EZH2/MEK inhibitors triggered potent tumor regression (Fig. 2A–J) with no observed toxicity or weight loss (Supplementary Fig. S2A–S2E). Specifically, the LOVO xenograft model regressed up to 75% (Fig. 2A), whereas the PDX models (COCA74P, COCA9, COCA4, and COCA30) regressed up to 74%, 54%, 48%, and 72%, respectively, over 4 weeks (Fig. 2C, E, G, and I).

While longer treatment was not possible because of the need for repeated oral gavaging (3×/day), mice harboring COCA74P tumors were followed up after treatment ended at 28 days. Animals exposed to vehicle, trametinib, or tazemetostat alone died relatively quickly (median survival 42, 48, and 46 days, respectively); however, survival was substantially increased in mice treated with both agents together, despite the cessation of treatment (median survival 77 days; Fig. 2K).

EZH2 and MEK Inhibitors Cooperatively Induce the Expression of Intestinal Differentiation Markers

We also evaluated the therapeutic efficacy of these agents in organoids derived from previously characterized genetically engineered mouse models with mutations in *Apc*, *Kras*, and *Trp53* (termed AKP) or *Apc*, *Kras*, *Trp53*, and *Tgfb1* (termed AKPT; refs. 33, 34). Similar to cell line studies, tumor organoids were pretreated with EZH2 inhibitor for 5 to 7 days, prior to the addition of MEK inhibitor. Interestingly, a subset of organoids treated with the EZH2 inhibitor adopted a branched, gut-like morphology, reminiscent of differentiated organoids grown in WNT-depleted media (Fig. 3A; ref. 35). Additionally, whereas the MEK inhibitor reduced proliferation in both models, only the combination triggered cell death as illustrated by a rapid decrease in cell number (Fig. 3B; Supplementary Fig. S3A). Human tumor organoids derived from a *KRAS*^{G12D}-mutant tumor similarly died in response to these agents (Supplementary Fig. S3B).

Based on these interesting morphological changes, we considered the possibility that EZH2 inhibition might be functioning by promoting a shift in the differentiation state. To investigate this possibility, RNA sequencing (RNA-seq) was performed using multiple human colorectal cancer cell lines treated with EZH2 and/or MEK inhibitors or EZH2 and *KRAS*^{G12D} inhibitors. mRNA was collected 16 hours after treatment with the combination, prior to the onset of substantial cell death. Single sample gene set enrichment analysis (ssGSEA) revealed that many genes associated with markers of differentiated intestinal cell types (enterocytes, enteroendocrine cells, goblet cells, deep crypt secretory cells, and tuft cells) were upregulated by these agents (Fig. 3C; Supplementary Fig. S3C; refs. 36, 37). Surprisingly, however, we found that both agents contributed to this response. Notably, the signatures that were most cooperatively upregulated were associated with goblet cells, tuft cells, and enteroendocrine cells, suggesting that EZH2 and MEK inhibitors preferentially drive differentiation toward a secretory lineage. Concomitantly, signatures associated with intestinal stem cells decreased (Fig. 3C; Supplementary Fig. S3C; ref. 38). Although the relative contribution of each agent on specific signatures varied

between cell lines, in all cases both agents were required for a maximal shift in the differentiation state. This dramatic shift in gene expression was further confirmed by immunoblotting (Fig. 3D; fully quantified in Supplementary Fig. S3D). For example, well-established genes associated with differentiated intestinal cells, including *ATOH1*, *CDX2*, and *KRT20*, were upregulated 4.6- to 57.2-fold, whereas stem-like associated genes including *LGR5*, *SOX9*, and *PROM1* were downregulated, by 1.6- to 124.2-fold (Fig. 3D; ref. 39). Consistent with RNA-seq data, the relative contribution of each agent to the induction or suppression of different markers varied, but overall, both agents were required for a maximal response.

Suppression of WNT Signaling and Induction of Differentiation Are Required for Cell Death

The WNT pathway plays a critical role in the self-renewal and maintenance of intestinal epithelial cells (40, 41). Moreover, suppression of WNT signaling has been shown to induce differentiation and promote tumor regression in various animal models of colorectal cancer (42–45). Therefore, we investigated whether these agents were suppressing oncogenic intestinal WNT transcriptional signatures (46, 47). ssGSEA of multiple oncogenic intestinal WNT pathway signatures further revealed that, like intestinal differentiation genes, both agents were required for maximal suppression of the pathway (Fig. 3E). Similar cooperative suppressive effects were observed in the *KRAS*^{G12D} cells treated with EZH2/*KRAS*^{G12D} inhibitors (Supplementary Fig. S3E). These data suggest that EZH2 and RAS pathway inhibitors also cooperatively suppress WNT-driven transcription.

However, to determine whether suppression of oncogenic intestinal WNT signaling was required for cell death in response to EZH2 and MEK inhibitors, colorectal cancer cells were transduced with a constitutively active form of β -catenin, lacking the first N-terminal 90 amino acids that encode critical regulatory sequences (β -catenin Δ 90; ref. 48). Importantly, β -catenin Δ 90 restored the expression of oncogenic intestinal WNT signatures in cells treated with the combination (Fig. 3F, expression shown in Supplementary Fig. S3F). Moreover, its expression blocked the enhanced apoptosis triggered by EZH2/MEK inhibitors (Fig. 3G) and the subsequent depletion of cells in multiple models (Fig. 3H; Supplementary Fig. S3G), demonstrating that suppression of the WNT/ β -catenin pathway is functionally required for cell death. Of note, MEK and EZH2 inhibitors are also known to independently affect the expression of various cell cycle regulators, including p21, p27, and cyclin D1, which we observed (Supplementary Fig. S3H; ref. 49). Accordingly, these agents also cooperatively activated the RB pathway (Supplementary Fig. S3I and S3J), which was not restored by β -catenin Δ 90 reconstitution (Supplementary Fig. S3I and S3J). Therefore, we conclude that WNT pathway suppression is required for cell death triggered by combined EZH2 and MEK inhibitors; however, these agents can also restrict the proliferation of any remaining cells through additional mechanisms likely affecting multiple cell-cycle regulators.

Finally, we investigated whether blocking intestinal differentiation might also prevent cell death. As noted, we observed that *CDX2*, an intestinal-specific homeobox gene

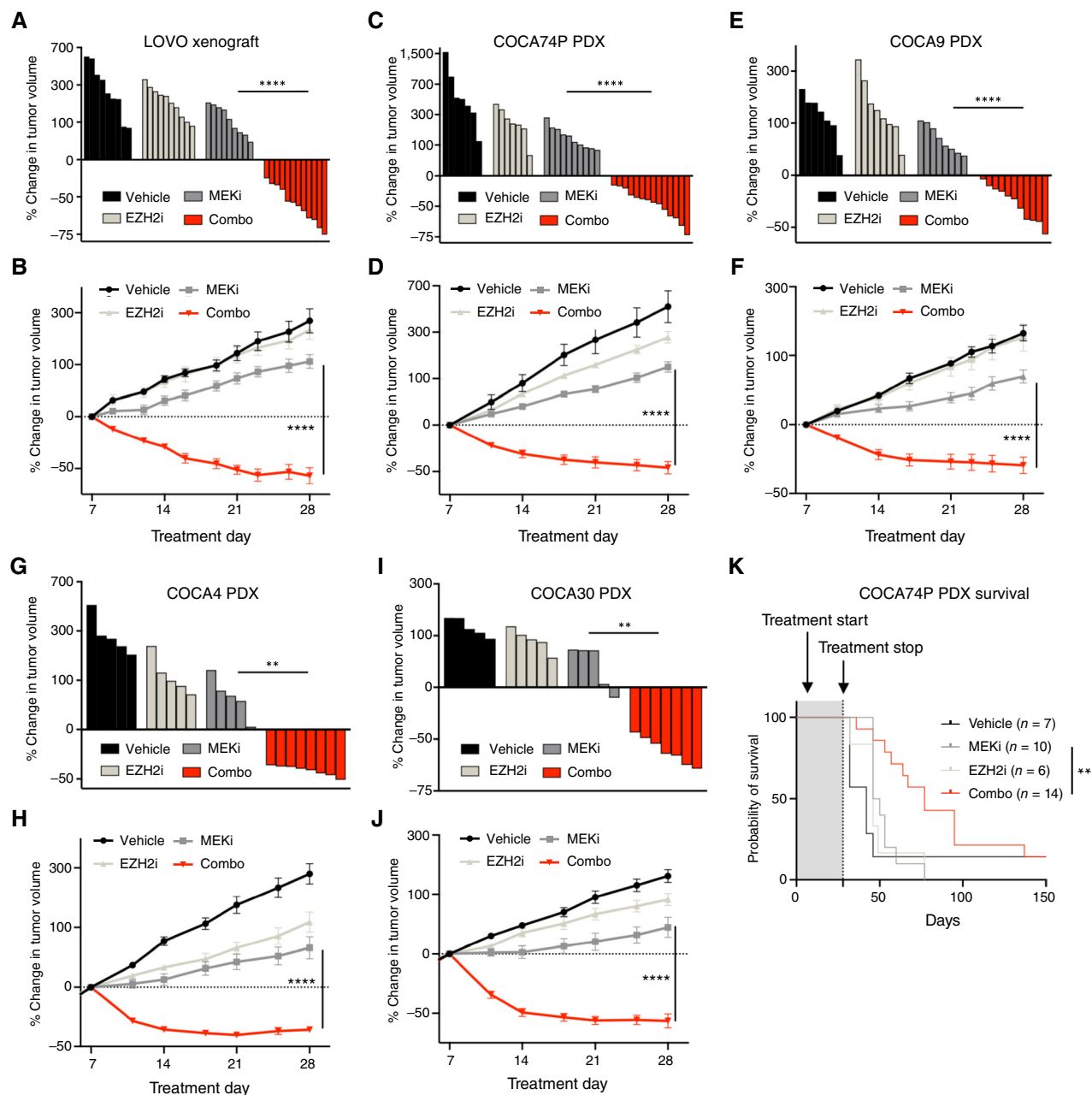


Figure 2. Combined suppression of EZH2 and the RAS pathway promotes tumor regression in multiple *in vivo* models and enhances survival. **A–J**, Top, waterfall plots depict change in tumor volume in KRAS-mutant colorectal cancer xenograft model LOVO (**A** and **B**), COCA74P colorectal cancer PDX (**C** and **D**), COCA9 colorectal cancer PDX (**E** and **F**), COCA4 colorectal cancer PDX (**G** and **H**), or COCA30 colorectal cancer PDX (**I** and **J**) at day 28, after 21 days of treatment with vehicle, EZH2i (tazemetostat), and/or MEKi (trametinib). Each bar represents an individual tumor. Bottom, Graphs depict maximal change in tumor volume over time compared with day 7 at the start of MEKi/vehicle treatment. Each data point represents mean \pm SEM of individual tumors shown in **A**, **C**, **E**, **G**, and **I**. In all models, tumors were implanted subcutaneously, and established tumors were pretreated for 7 days with vehicle or EZH2i (tazemetostat) prior to treatment with additional vehicle, MEKi, and/or EZH2i treatment starting at day 7, for a total of 28 days. Axis depicts percent change in tumor volume. ****, P value < 0.0001 determined using Mann–Whitney test between MEKi- and combo-treated arms. **, Kaplan–Meier survival curve of COCA74P PDX mice treated with vehicle, MEKi (trametinib), and/or EZH2i (tazemetostat). MEKi vs. combo P = 0.002 via log rank test. Median survival for vehicle, MEKi, EZH2i, and combo is 42, 48, 46, and 77 days, respectively.

known to be critical for intestinal differentiation, was potentially upregulated by these agents (50). Importantly, siRNA-mediated suppression of *CDX2* also prevented the cytotoxic effects of the combination (Fig. 3I, knockdown shown in Supplementary Fig. S3K). Conversely, expression

of *SOX9* has been shown to drive a stem cell-like program that blocks intestinal differentiation in colorectal cancer (51). Accordingly, ectopic expression of *SOX9* was also able to prevent cell death in response to these agents (Fig. 3J, expression shown in Supplementary Fig. S3L). Taken together,

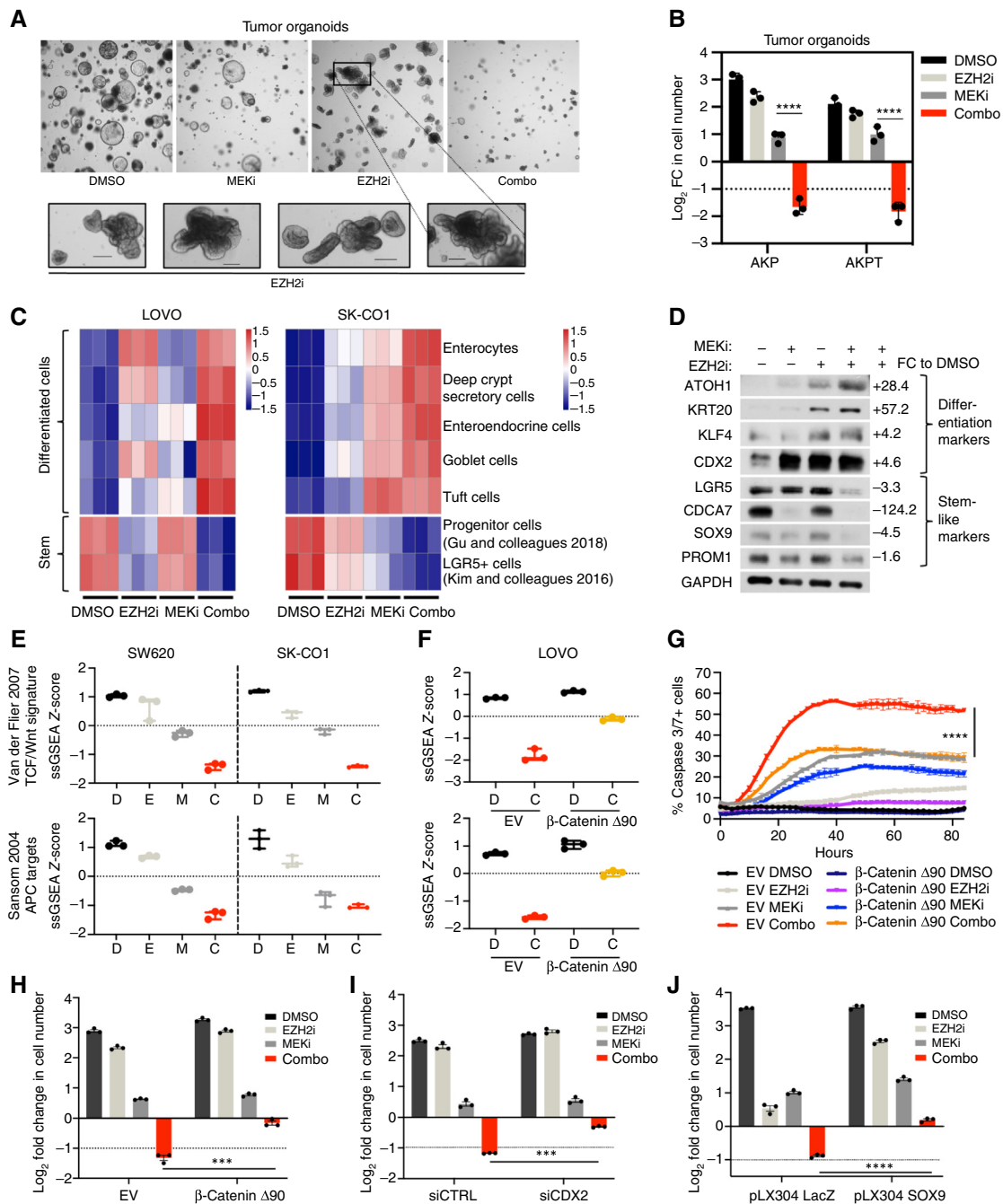


Figure 3. EZH2 and MEK inhibitors cooperatively suppress WNT signaling and drive differentiation. **A**, Representative images of vehicle-, MEKi-, EZH2i-, and combo-treated AKP tumor organoids 24 hours after combination treatment (6 days after EZH2i pretreatment). Magnification shown for EZH2i-treated organoids. Scale bars, 150 μ m. **B**, Proliferation assay for AKP and AKPT tumor organoids after treatment with the indicated compounds for 3 days. **C**, ssGSEA of signatures associated with differentiated cell types using RNA-seq from LOVO and SK-CO1 cell lines treated with EZH2i and/or MEKi. Signatures composed of combined gene lists as described in refs. 35, 36. **D**, Immunoblot of LOVO protein lysates from cells treated with EZH2i and/or MEKi depicting expression of several proteins associated with differentiated intestinal cells (ATO1, KRT20, KLF4, and CDX2) and stem cells (LGR5, SOX9, PROM1, and CDCA7). pERK and H3K27me3 indicate MEKi and EZH2i target inhibition, and ERK, Histone H3, and GAPDH are loading controls. Quantification indicates fold change (FC) compared with DMSO. **E** and **F**, Plots depicting ssGSEA z-scores of signatures associated with oncogenic intestinal Wnt signaling from RNA-seq data in (E) SW620 and SK-CO1 cells or (F) LOVO cells transduced with an empty vector or a construct to express a constitutively active form of β -catenin after treatment with the indicated agents (C, combination; D, DMSO; E, tazemetostat; M, trametinib). **G**, Caspase 3/7+ cells (apoptotic) after treatment with EZH2i and/or MEKi in LOVO cells expressing empty vector or β -catenin Δ 90 as measured by Incucyte live-cell imaging. *P* value determined with two-way ANOVA between empty vector and β -catenin Δ 90 transduced combo-treated cells. **H**, Proliferation of LOVO pLV β -catenin Δ 90 cells treated with MEKi and/or EZH2i for 5 days. **I**, Proliferation of LOVO cells transfected with siRNAs against a control sequence or CDX2 and then treated with MEKi and/or EZH2i for 5 days. **J**, Proliferation of SK-CO1 cells transduced with lentivirus to express LacZ or SOX9 and then treated with MEKi and/or EZH2i for 5 days. Unless otherwise indicated, for all subfigures bars represent mean \pm SD of technical replicates. *P* value measured by unpaired *t* test. *, *P* < 0.05; **, *P* < 0.01; ***, *P* < 0.001; ****, *P* < 0.0001.

these data demonstrate that suppression of oncogenic WNT signaling and the induction of intestinal differentiation programs are required for the therapeutic response to EZH2 and MEK inhibitors.

Co-suppression of EZH2 and RAS Signaling Selectively Drives Differentiation of Tumors *In Vivo*

Given the dramatic effects of these agents on differentiation markers *in vitro*, we investigated whether these changes were also occurring *in vivo*. Combined EZH2/MEKi triggered a rapid and progressive increase in mucinous cells in CDX tumors, which could be readily observed by gross histologic analysis of hematoxylin and eosin-stained sections within 1 to 4 days (Fig. 4A). Cyclic immunofluorescence (CyclIF) revealed that this was accompanied by a dramatic decrease in SOX9 expression and a concomitant increase in CDX2 expression (red→green; Fig. 4A). A similar shift in the differentiation state was observed in PDX tumors, which also adopted a mucinous appearance, along with a reduction in SOX9 and increase in KRT20 (red→green; Fig. 4B). Whereas frank tumor regression could be readily measured within 3 days (Fig. 2A–I), drug-induced PARP cleavage could not be accurately quantified in tumor cells *in vivo* because of the high baseline levels of necrosis in these models and the progressive nature of cell death and clearing.

Consistent with the absence of weight loss, no changes in the expression patterns of CDX2, KRT20, and SOX9 were observed in the mouse colons even after long-term treatment with EZH2 and MEK inhibitors (Fig. 4C). A slight suppression of pERK in normal colon was observed (Supplementary Fig. S4A and S4B), but Ki67 levels did not change (Fig. 4D). These findings suggest that a therapeutic window can be achieved between KRAS-mutant/EZH2-overexpressing colorectal cancers and normal tissue. Although toxicity in humans can only be determined empirically, the observation that these agents do not affect body weight, body score, or colonic differentiation is promising. Indeed, a clinical trial evaluating tazemetostat with dabrafenib/trametinib in metastatic melanoma is underway (NCT04557956).

EZH2 and MEK Inhibitors Mediate Their Effects by Upregulating the WNT Pathway Repressor TLE4

EZH2 functions by inhibiting the expression of specific genes, through the deposition of repressive H3K27me3 marks. Therefore, to identify de-repressed EZH2 targets required for this response, CUT&RUN analysis was performed on LOVO cells treated with EZH2 and MEK inhibitors using H3K27me3 antibodies. We first identified *bona fide* EZH2 targets by integrating RNA-seq and CUT&RUN data and found that 2,356 genes were differentially upregulated by the combination, 2,911 genes had differentially lost H3K27me3 binding at promoter regions, and 573 genes were upregulated and lost H3K27me3 binding, representing potential EZH2 targets of interest (Fig. 5A). These targets were further reduced to 299 genes by identifying those that were also transcriptionally upregulated in a second colorectal cancer cell line, SW620.

Among these 299 targets, we prioritized those implicated in colonic or intestinal differentiation or with a proposed tumor suppressive function and enriched this list for transcription factors, which could have broad reprogramming effects. We then initiated a screen to identify genes that were required for cell death in response to EZH2/MEK inhibitors by suppressing each gene individually with pooled siRNA sequences. Strikingly, a hit that blocked the cytotoxic effects of the combination by ≥75% (when suppressed) was identified within the first panel of 15 genes: the *TLE4* gene (Fig. 5B, knock-down shown in Supplementary Fig. S5A). Two independent Clustered Regularly Interspaced Short Palindromic Repeats (CRISPR) guide sequences confirmed the requirement for *TLE4* in the cytotoxic response to EZH2 and MEK inhibitors (Fig. 5C and D; Supplementary Fig. S5B). Immunoblots further demonstrated that the TLE4 protein is potently upregulated by these agents by 5.48-fold (Fig. 5D, quantified in Supplementary Fig. S5C). As expected, EZH2 inhibition exerted a dominant effect on TLE4 expression levels; however, we noted that MEK inhibitors slightly enhanced its expression (Fig. 5D, quantified in Supplementary Fig. S5C).

TLE4 suppression prevented the dramatic loss of cells in multiple cell lines (Fig. 5B and E) and suppressed the enhanced apoptosis triggered by the combination (Supplementary Fig. S5D). Of note, *TLE4* ablation had no effect on RAS/ERK signaling. In colorectal cancer models, trametinib rapidly suppresses pERK; however, it becomes partially reactivated within 24 to 48 hours (Supplementary Fig. S5E), which is thought to contribute to its lack of efficacy. As mentioned previously but shown here in more detail, tazemetostat did not further suppress RAS signaling or prevent the rebound of pERK in response to trametinib (Supplementary Fig. S5F). *TLE4* ablation also had no effect on pERK levels (Supplementary Fig. S5F). Together these findings demonstrate that EZH2 inhibition does not potentiate the therapeutic effects of RAS pathway inhibitors by further suppressing RAS signaling and that *TLE4* ablation does not rescue these effects by restoring or enhancing RAS signaling.

Most importantly, *TLE4* ablation prevented tumor regression *in vivo* induced by these agents (Fig. 5F). Consistent with additional known effects on cell-cycle components (Supplementary Fig. S3H–S3J), EZH2 inhibitor and MEK inhibitor (EZH2i/MEKi) was still able to confer cytostasis in the absence of TLE4, similar to observations in *in vitro* β-catenin Δ90 and SOX9 reconstitution studies (Fig. 3H–J). Thus, *TLE4* upregulation is required for apoptosis and the full therapeutic response to EZH2 and MEK inhibitors, but surviving tumor cells can be further restrained by additional mechanisms likely affecting cell-cycle components.

TLE4 is a member of the TLE family of transcriptional repressors involved in the negative regulation of canonical WNT signaling (52). When WNT signaling is active, β-catenin translocates to the nucleus and associates with TCF/LEF factors to drive the transcriptional activity of WNT-responsive targets. However, transcription can be suppressed by Groucho/TLE repressive complexes that competitively associate with TCF/LEF factors (53), providing a potential link between *TLE4* induction and WNT pathway suppression in this setting. CUT&RUN analysis further demonstrated that H3K27me3 was bound throughout the

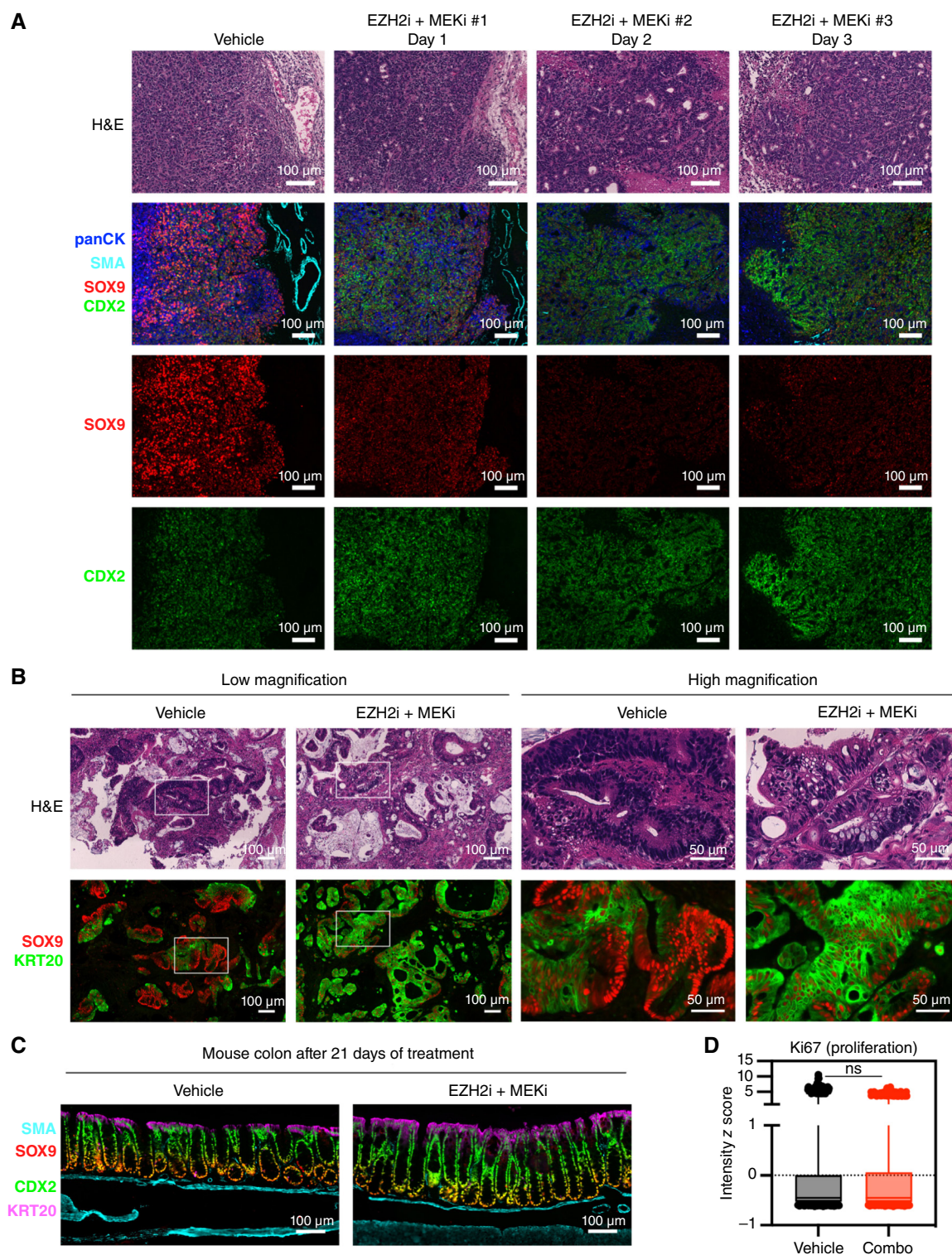


Figure 4. Co-suppression of EZH2 and RAS signaling selectively drives differentiation of tumors *in vivo*. **A**, Histological (H&E) and multiplexed immunofluorescent (CyCIF) imaging of cell line-derived xenograft LOVO tumors treated with vehicle or EZH2i for 7 days followed by EZH2i + MEKi for 1, 2, or 3 additional days. Imaging was conducted using antibodies against SMA (cyan; structural), panCK (blue; epithelial), SOX9 (red; stem-like), and CDX2 (green; differentiated) in merged or single channel images as indicated. **B**, Same as **A**, but using PDX COCA30 tumors treated with vehicle or EZH2i for 7 days followed by EZH2i + MEKi for 1 additional day. Low- and high-magnification images are shown. **C**, Multiplexed immunofluorescent imaging (CyCIF) of colon tissue from tumor bearing mice after 21 days of treatment with vehicle or EZH2i + MEKi stained with antibodies for SMA (cyan; structural), Hoechst (blue; nuclei), SOX9 (red; stem-like), CDX2 (green; differentiated), and KRT20 (magenta; differentiated). **D**, Quantification of Ki67 intensity in cellular compartment of colons described in **C**. H&E, hematoxylin and eosin.

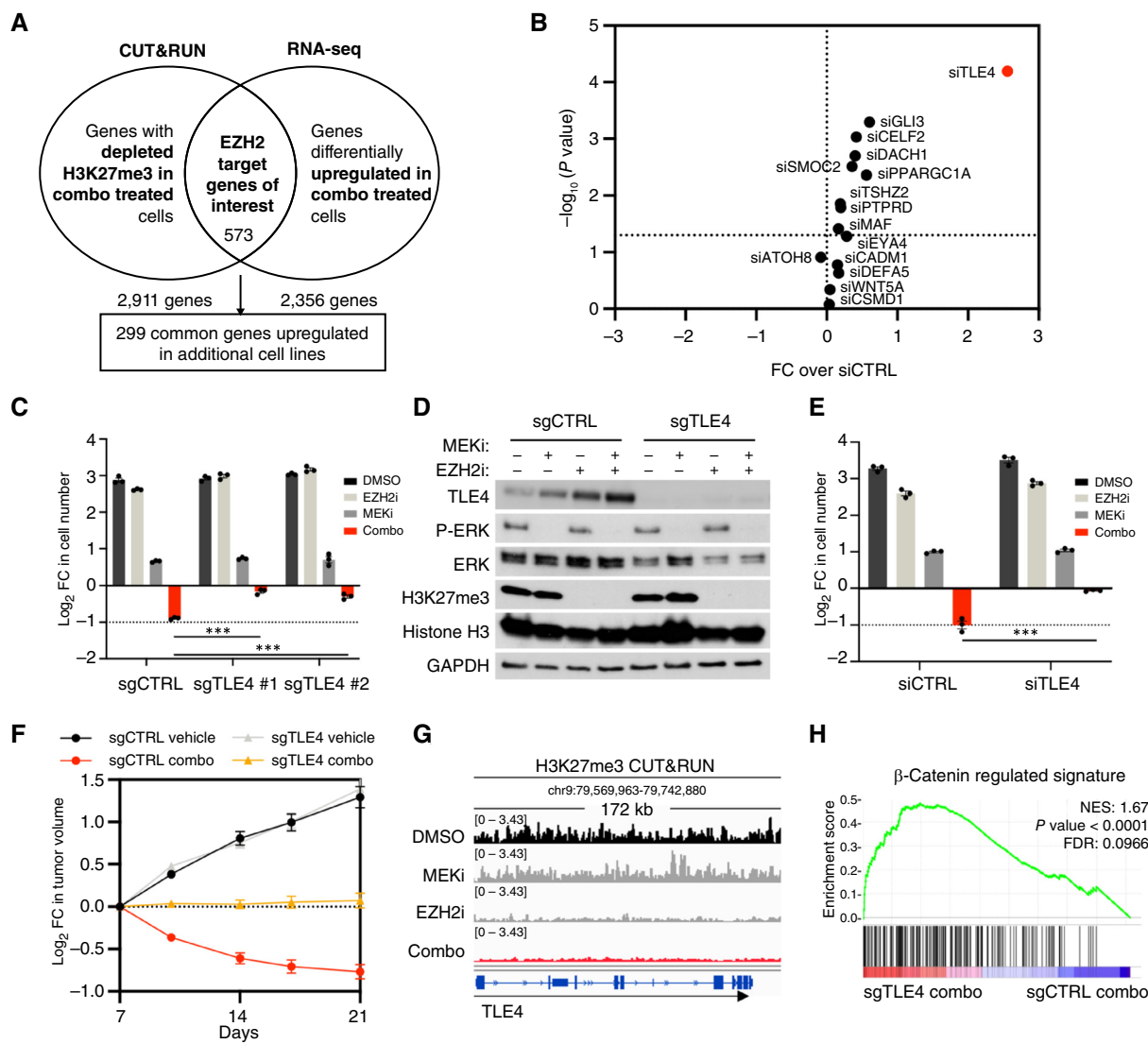


Figure 5. Induction of the WNT pathway repressor *TLE4* contributes to the therapeutic response. **A**, Venn diagram schematic of the number of candidate genes overlapping from CUT&RUN (differential loss of H3K27me3 between combo and DMSO) and RNA-seq [$>1 \log_2$ fold change (FC) increase between combo and DMSO] in LOVO and SW620 cell lines after filtering for statistical significance ($P_{adj} < 0.05$, $FDR < 0.05$). **B**, Proliferation assays were conducted in LOVO cells transfected with the indicated siRNAs and then treated with DMSO or a combination of MEKi and EZH2i. Volcano plot depicts relative FC in cell number compared with siCTRL and P value after 5 days of drug treatment after siRNA transfection. **C**, Proliferation assay in LOVO cells transfected with sgRNAs against a control sequence, or two different targeting sequences against *TLE4*, and then treated with MEKi and/or EZH2i using indicated antibodies. **D**, Immunoblot of LOVO cells transfected with sgRNAs against a control sequence or *TLE4* (guide #1) and then treated with MEKi and/or EZH2i using indicated antibodies. **E**, Proliferation of SW620 cells transfected with siRNAs against a control sequence or *TLE4* and then treated with MEKi and/or EZH2i for 5 days. **F**, In vivo xenograft assay with mice injected with LOVO sgCTRL or sg*TLE4* cells and subsequently treated with vehicle or combination of EZH2 and MEK inhibitors. Graphs depict change in tumor volume over time compared with day 7 at the start of MEKi/vehicle treatment. Each data point represents mean \pm SEM of individual tumors. ****, P value < 0.0001 determined using Mann-Whitney test between sgCTRL and sg*TLE4* combo-treated arms. **G**, Histogram depicting H3K27me3 in LOVO cells treated with indicated compounds from CUT&RUN experiment. Genome view depicts *TLE4* gene body. **H**, GSEA leading edge plot depicting enrichment of β -catenin-regulated signature in sg*TLE4* combo treated cells vs. sgCTRL combo-treated cells. Unless otherwise indicated, for all subfigures bars represent mean \pm SD of technical replicates. P value measured by unpaired t test. *, $P < 0.05$; **, $P < 0.01$; ***, $P < 0.001$; ****, $P < 0.0001$.

entire *TLE4* gene in colorectal cancer cells and showed that binding was lost in response to EZH2 inhibitor alone or the combination (Fig. 5G), suggesting that EZH2 inhibitors control the expression of *TLE4* by removing repressive H3K27me3 marks at the *TLE4* locus. Moreover, analysis of transcriptional profiles from colorectal cancer cells with and without *TLE4* demonstrated that *TLE4* ablation partially restored the

expression of β -catenin-regulated genes in these cells (Fig. 5H). Together, these findings suggest that *TLE4* is a critical PRC2 target in colorectal cancers, its de-repression is required for the therapeutic response to EZH2 and MEK inhibitors, and its induction contributes to the WNT pathway suppression. Nevertheless, we expected that additional genes were likely contributing to this response.

Downloaded from <http://aacrjournals.org/cancerdiscovery/article-pdf/14/12/2430/351937/1.cd-23-0866.pdf> by guest on 29 April 2025

EZH2 and RAS Pathway Inhibitors Cooperatively Upregulate PRC2 Targets and Induce Additional WNT Suppressive/Differentiation Genes

In the course of this analysis, we noted that tazemetostat alone increased the expression of genes in which H3K27me3 binding was lost at proximal regulatory sites, as expected [Fig. 6A (third vs. first column)]. Surprisingly, however, trametinib substantially enhanced the effects of tazemetostat, resulting in the *de novo* or cooperative upregulation of the majority of PRC2 targets [275 and 259 genes, respectively; Fig. 6A (last column)]. Gene Ontology (GO) term analysis revealed that signatures associated with WNT suppression, differentiation, and development were significantly enriched in this list of 534 *de novo*/cooperatively upregulated PRC2 targets (Fig. 6B), suggesting that combined EZH2 and MEK inhibitors might be exerting broader suppressive effects on these pathways. Notably, the same cooperative upregulation of PRC2 targets was observed in cells treated with KRAS^{G12D} and EZH2 inhibitors (Supplementary Fig. S6A and S6B).

An unbiased assessment of GO terms associated with these 534 genes indicated that many were components of WNT pathway suppression, cell differentiation, or developmental process signatures (Fig. 6B). Notably, multiple known negative regulators of the Wnt/ β -catenin pathway were among the uniquely induced PRC2 targets, although many function upstream of APC (e.g., *DKK3*, *SFRP4*, *WIF1*, and *FRZB*; Fig. 6C). Therefore, although potentially important in tumors with wild-type APC, the induction of these genes might not be expected to contribute to WNT pathway suppression in our models, which harbor APC mutations. However, we identified some genes (e.g., *TRPS1* and *SOX6*) which were also present in this list and have been proposed to exert more direct suppressive effects on β -catenin (54, 55). In addition, we noted that *ATOH1*, a transcription factor known to promote differentiation into the secretory lineage, was also cooperatively induced by EZH2 and MEK inhibitors (Fig. 6C; ref. 56). To determine whether upregulation of these genes might also contribute to the therapeutic response, they were individually ablated using siRNA pools, and cells were treated with EZH2 and MEK inhibitors as described in Fig. 5B. Notably, the ablation of *TRPS1*, *SOX6*, and to a lesser extent *ATOH1* all reduced the cytotoxic response to EZH2 and MEK inhibitors (Fig. 6D; knockdown shown in Supplementary Fig. S6C–S6E). Similar observations were made in two additional colorectal cancer cell lines, with some variation in the degree of rescue of each component, as might be expected (Fig. 6E and F; Supplementary Fig. S6E–S6I). Although we were unable to effectively ablate all three components simultaneously, each of them has been implicated in WNT pathway suppression and/or differentiation, and future studies will be required to understand their precise function. Together these observations demonstrate that TLE4 is a critical PRC2 target that suppresses WNT/ β -catenin-driven transcription and mediates the therapeutic response; however, these agents cooperatively induce a larger network of genes that suppress the WNT pathway and/or promote differentiation, which could be further investigated in future studies.

Apoptosis Is Mediated by the Cooperative Induction of the Proapoptotic Protein BMF

These data indicated that EZH2 and MEK inhibitors cooperatively suppress WNT/ β -catenin signaling and drive differentiation, which are required for cell death. However, ectopic expression of *TLE4* or genetic ablation of β -catenin was not sufficient to trigger the acute loss of cells alone or when combined with MEK inhibitors (Supplementary Fig. S7A and S7B). Therefore, we also sought to identify specific apoptotic regulators involved in this process. Indeed, EZH2 and MEK inhibitors also cooperatively upregulated genes associated with apoptosis (Fig. 7A). Strikingly, analysis of the differentially expressed genes after EZH2/MEK inhibition revealed that the proapoptotic gene *BMF* was induced ≥ 30 -fold and was the most significantly upregulated gene on this list (Fig. 7B). CUT&RUN analysis further revealed that, whereas H3K27me3 binding was relatively low at the *BMF* promoter and the gene body, broad H3K27me3 peaks were present at sequences immediately upstream, which were lost in response to EZH2 inhibition, consistent with a suppressive role for PRC2 at these sequences (Fig. 7C). Similar to the PRC2 targets shown in Fig. 6A, inhibition of both EZH2 and MEK was required for its maximal induction, which was observed in multiple colorectal cancer cell lines (Fig. 7D).

BMF is a BH3-only protein that acts as an apoptotic sensitizer by binding and sequestering antiapoptotic proteins including BCL-2, BCL-xL, and MCL-1 (57, 58). Importantly, we found that RNAi-mediated suppression of the *BMF* gene inhibited the robust loss of cells triggered by EZH2 and MEK inhibitors in multiple cell lines (Fig. 7E). *BMF* inhibition also suppressed apoptosis triggered by these agents (Supplementary Fig. S7C). Because *BMF* antibodies are of poor quality, we introduced a hemagglutinin tag (HA) epitope into the endogenous *BMF* locus via a CRISPR/Cas9 approach into LOVO and SW620 cells (57). Immunoblots illustrate the potent upregulation of the endogenous (tagged) protein and its effective knockdown by pooled siRNA sequences in both cell lines (Fig. 7F; Supplementary Fig. S7D). Knockdown was confirmed in other cell lines by qPCR (Supplementary Fig. S7E and S7F). Notably, these responses could be recapitulated by CRISPR/Cas9 sgRNA-mediated ablation of *BMF* (Fig. 7G and H; Supplementary Fig. S7G), which also prevented tumor regression *in vivo* (Fig. 7I). Interestingly, we found that *SOX9* expression and *CDX2* ablation, both which block differentiation and inhibit the cytotoxic response as shown in Fig. 3I and J, did not prevent the upregulation of *BMF* (Supplementary Fig. S7H and S7I). Taken together, these findings demonstrate that EZH2 and RAS pathway inhibitors independently drive differentiation and upregulate *BMF* and that both are required for cell death. This also suggests that a more differentiated state is required for *BMF* to exert its apoptotic effects. A model summarizing all of these data is shown in Fig. 7J.

DISCUSSION

Here, we report a promising therapeutic strategy for KRAS-mutant colorectal cancers, one of the most treatment-refractory subtypes of this disease. Specifically, we have shown that EZH2 and RAS pathway inhibitors potently synergize, trigger apoptosis, and induce dramatic tumor regression in

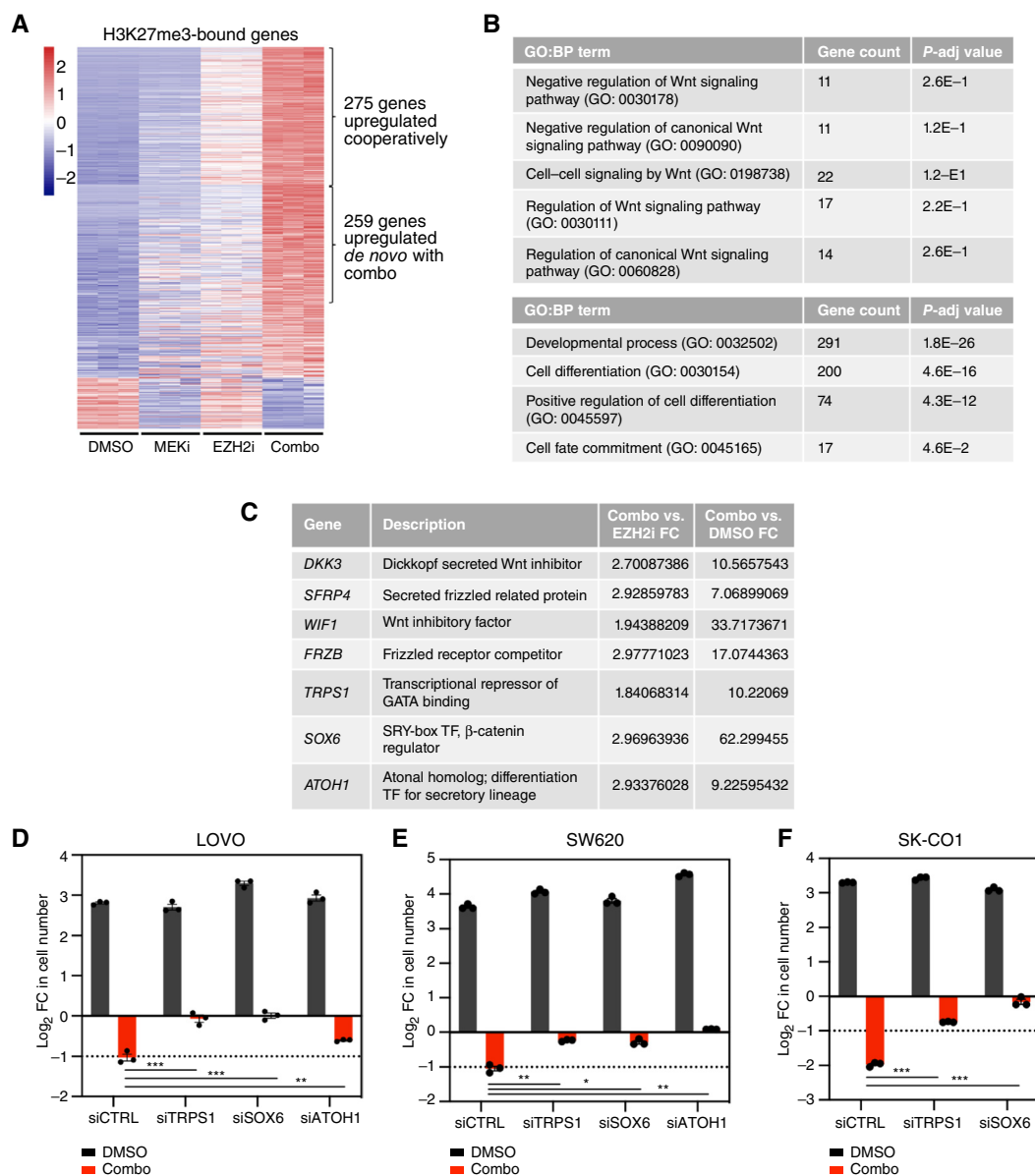


Figure 6. EZH2 and RAS pathway inhibitors cooperatively upregulate PRC2 targets and induce additional WNT suppressive/differentiation genes. **A**, Transcriptional heatmap of LOVO cells showing relative mRNA levels (P adj < 0.05, base means >10) of PRC2 targets as defined by differential loss of H3K27me3 from CUT&RUN experiments after treatment with DMSO, MEKi, and/or EZH2i [*de novo* upregulation = 275 genes as defined by DMSO \log_2 FC >1 and EZH2i vs. DMSO \log_2 FC <1; and cooperatively upregulated = 259 genes as defined by both combo vs. DMSO and EZH2i vs. DMSO > 1, with a difference >0.5]. **B**, Table depicting GO:BP terms associated with negative regulation of WNT signaling pathways (top) and differentiation (bottom) that are significantly enriched in the 534 *de novo*/cooperatively upregulated PRC2 targets. **C**, Table listing some cooperatively upregulated PRC2 genes that impinge on WNT and differentiation pathways. Combo vs. EZH2i FC and combo vs. DMSO FC are shown to highlight the additional effects of adding trametinib on their expression. **D–F**, Proliferation of LOVO cells in **D**, SW620 cells in **E**, and SK-CO1 cells in **F** transfected with the indicated siRNAs and then treated with DMSO or a combination of MEKi and EZH2i for 5 days. Mean \pm SD of technical replicates; P value measured by unpaired t test between combo-treated conditions. *, P < 0.05; **, P < 0.01; ***, P < 0.001.

multiple PDX tumor models, including a model derived from a previously treated colorectal cancer metastasis. We further demonstrate that these agents function by cooperatively driving differentiation and inducing the expression of *BMF*, a proapoptotic Bcl-2 family member. Genetic studies indicate that both processes are required for cell death, suggesting that cells in a more differentiated state are more sensitive to this apoptotic signal.

These effects are mediated, in part, by the induction of *TLE4*, a member of the TLE/Groucho family of transcriptional repressors, which play a well-established role in repressing WNT/ β -catenin-regulated transcription. We show that *TLE4* is a *bona fide* PRC2 target gene and is decorated with repressive H3K27me3 marks in colorectal cancer cells. Accordingly, the induction of *TLE4* requires the loss of H3K27me3, conferred by EZH2 inhibition. Unexpectedly however, we discovered that

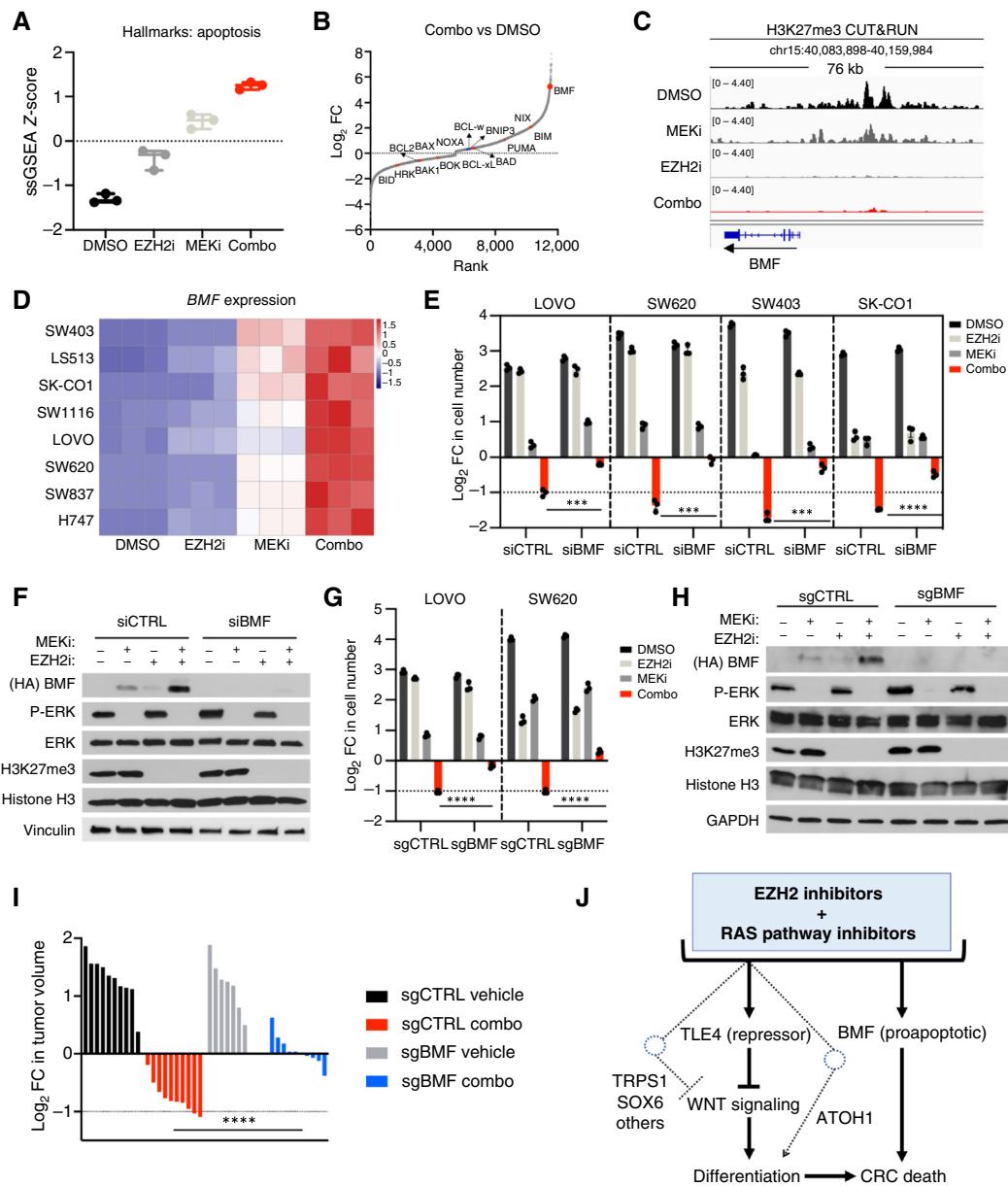


Figure 7. Apoptosis is mediated by the cooperative induction of the proapoptotic protein BMF. **A**, ssGSEA z-scores of Hallmarks: apoptosis signature from RNA-seq data in LOVO cell lines treated with MEKi and/or EZH2i, $n = 3$. **B**, Plot depicting all differentially expressed genes ($P \text{ adj} < 0.05$) between combo and DMSO treatment in LOVO cells by \log_2 fold change (FC) and rank from the most differentially downregulated gene to the most differentially upregulated gene. Proapoptotic BCL2 family members are depicted in red, and antiapoptotic BCL2 family members are depicted in blue. BMF is the most significantly differentially expressed BCL2 family member gene in combo-treated cells. **C**, Histogram depicting H3K27me3 in LOVO cells treated with indicated compounds using CUT&RUN. Genome section depicts BMF locus and genomic regions upstream. **D**, Transcriptional heatmap depicting relative z-score normalized mRNA levels of BMF in the indicated cell lines after treatment with DMSO, MEKi, and/or EZH2i. Heatmap rows represent mRNA levels obtained from RNA-seq experiments (LS513, SW620, SK-CO1, and LOVO) and mRNA levels obtained from qRT-PCR using BMF primers (SW403, SW1116, SW837, and H747). **E**, Left, Proliferation of LOVO, SW620, SW403, and SK-CO1 cells transfected with siRNAs against a control sequence or BMF, and then treated with MEK and/or EZH2i for 5 days. **F**, Immunoblot of LOVO protein lysates with stable HA knockin at endogenous BMF locus transfected with siRNAs against a control sequence or BMF and then treated with MEKi and/or EZH2i after 16 hours. **G**, Proliferation of LOVO and SW620 cells transfected with sgRNAs against a control sequence or BMF and then treated with MEKi and/or EZH2i for 5 days. **H**, Same as **F**, but cells were transfected with siRNAs against a control sequence or BMF. **I**, *In vivo* xenograft assay with mice injected with LOVO sgCTRL or sgBMF cells and subsequently treated with vehicle or combination of EZH2i (tazemetostat) and MEKi (trametinib). Waterfall plots depict maximal change in tumor volume after 14 days of treatment with vehicle or a combination of EZH2i and MEKi inhibitors. Each bar represents an individual tumor. ****, $P \text{ value} < 0.0001$ determined using Mann-Whitney test between sgCTRL and sgBMF combo-treated arms. Note that the sgCTRL vehicle- and combo-treated tumors are identical to the sgCTRL tumors depicted in Fig. 5F as these studies were performed concomitantly. **J**, Model depicting the mechanism by which EZH2 and RAS pathway inhibitors trigger cell death through the parallel induction of differentiation and the potent upregulation of BMF, a proapoptotic regulator. Differentiation is driven by the de-repression of a network of EZH2 targets that suppress the WNT/ β -catenin pathway, including TLE4, and additional genes involved in intestinal differentiation. Unless otherwise indicated, for all subfigures, bars represent mean \pm SD of technical replicates. P value measured by unpaired t test. *, $P < 0.05$; **, $P < 0.01$; ***, $P < 0.001$; ****, $P < 0.0001$.

RAS pathway inhibitors cooperatively regulate the majority of PRC2 targets in colorectal cancers, triggering their induction but only when repressive H3K27me3 marks are lost in response to EZH2 inhibition. Interestingly, many of these genes also suppress the WNT pathway and/or promote intestinal differentiation, and we confirmed that a subset contributes to the therapeutic response. Finally, we show that EZH2 and RAS pathway inhibitors also converge on critical apoptotic signals via a similar mechanism, specifically the proapoptotic protein BMF. Taken altogether, these studies mechanistically reveal how EZH2 inhibitors epigenetically reprogram colorectal cancers and consequently transform the transcriptional response to RAS pathway inhibitors. This epigenetic reprogramming converts the relatively modest effects of RAS pathway inhibitors to a robust transcriptional response that drives WNT suppression, differentiation, and apoptosis in colorectal cancers.

Interestingly, suppression of WNT signaling has been shown to induce differentiation and promote tumor regression in various mouse models of colorectal cancer (42–45). Nevertheless, WNT pathway inhibition is not universally effective in all human cell line models (59). However, Dow and colleagues found that inhibition of CDK4, a distal downstream effector of the RAS pathway, could synergize with tankyrase inhibition in resistant models and induce cell-cycle arrest and senescence (59). Perhaps EZH2 and RAS pathway inhibitors are functioning in an analogous capacity, as we have shown here that EZH2 and RAS pathway inhibitors cooperatively suppress WNT signaling and activate RB. However, additional induction of the apoptotic regulator BMF, which specifically requires EZH2-mediated de-repression, may convert cytostatic effects to a cytotoxic response.

Many of the studies presented here describe the combined effects of EZH2 and MEK inhibitors, which could be broadly effective in colorectal cancers with all types of KRAS mutations. However, 8% and 33% of KRAS-mutant colorectal cancers harbor KRAS^{G12C} and KRAS^{G12D} mutations, respectively. As such, there is a great deal of enthusiasm for the newly developed KRAS^{G12C} and KRAS^{G12D} inhibitors in these settings. Indeed, EZH2 inhibitors similarly suppress WNT signaling, drive differentiation, and kill colorectal cancer cells when combined with these allele-selective inhibitors, providing important support for these combinations as well.

Altogether these studies have defined a promising therapeutic strategy for KRAS-mutant colorectal cancers, elucidated the mechanism by which these agents function, and uncovered important insight about how EZH2 and the RAS pathway cooperatively regulate the WNT pathway, differentiation, and survival/cell death in colorectal cancers. Indeed, the orthogonal activation/upregulation of RAS and EZH2 may provide a fail-safe mechanism for suppressing differentiation and apoptosis, which could underlie the treatment-refractory nature of KRAS-mutant colorectal cancers. Regardless, these findings have important clinical implications and provide strong mechanistic support for developing new clinical trials in colorectal cancers.

METHODS

Cell Lines and Reagents

All cell lines were purchased from ATCC. Cell lines were authenticated using short-tandem repeat profiling (Labcorp). All cell lines were regularly tested for *Mycoplasma* using the MycoAlert Mycoplasma

Detection Kit (Lonza, LT07-318). All cells were used for experiments within 10 to 15 passages from thawing. Cells were cultured in Ham's F-12 (Gibco, #11765), Eagle's minimum essential medium (Corning, #10-009-CV), DMEM (Corning, #10-013-CV), RPMI (Corning, #10-040-CV), or OptiMEM (Gibco, #31985), supplemented with FBS and 1× concentration of penicillin/streptomycin/glutamine (Gibco, #10378016). All cell lines were cultured with 10% FBS, except HIEC6 as specified by ATCC. Ten percent FBS was maintained during proliferation studies in all cell lines, except SW620 and SW837, in which 2% FBS was used starting at day 0. The precise concentration of trametinib used for proliferation studies in each cell line was determined by performing dose-response experiments to identify a cytostatic dose but not exceeding 50 nmol/L. Each cell line's culture media, mutation, and concentrations of trametinib and encorafenib are as follows: LS513 (RPMI, KRAS^{G12D}), and trametinib 5 nmol/L), SW403 (DMEM, KRAS^{G12V}, and trametinib 10 nmol/L), SW1116 (DMEM, KRAS^{G12A}, and trametinib 10 nmol/L), SK-CO1 (Eagle's minimum essential medium, KRAS^{G12V}, and trametinib 1 nmol/L), LOVO (Ham's F-12, KRAS^{G13D}, and trametinib 50 nmol/L), SW837 (DMEM, KRAS^{G12C}, and trametinib 50 nmol/L), SW620 (DMEM, KRAS^{G12V}, and trametinib 50 nmol/L), H747 (RPMI, KRAS^{G13D}, and trametinib 10 nmol/L), HIEC6 (OptiMEM + 4% FBS and trametinib 50 nmol/L), HT29 (McCoy's, BRAF^{V600E}, trametinib 5 nmol/L, and encorafenib 0.5 μmol/L), LS411N (RPMI, BRAF^{V600E}, trametinib 25 nmol/L, and encorafenib 2.5 μmol/L), COLO205 (RPMI, BRAF^{V600E}, trametinib 5 nmol/L, and encorafenib 1 μmol/L), COLO201 (RPMI, BRAF^{V600E}, trametinib 10 nmol/L, and encorafenib 1 μmol/L), KM12 (DMEM and trametinib 50 nmol/L), CACO2 (DMEM and trametinib 50 nmol/L), and SW48 (DMEM and trametinib 50 nmol/L).

Drugs were purchased from vendors: tazemetostat (SelleckChem, #S7128; used at 5 μmol/L), trametinib (LC Laboratories, #T8123), MRTX1113 (MedChemExpress; #HY-134813), MRTX849 (MedChemExpress; #HY-130149), binimetinib (SelleckChem, #S7007; used at 5 μmol/L), MAK683 (SelleckChem, #S8983; used 5 μmol/L), encorafenib (SelleckChem, #S7108), and cetuximab (SelleckChem, #A2000; used at 50 μg/mL).

Publicly Available Cancer Datasets

To determine EZH2 mRNA levels in colorectal cancer tumors and matched normal tissue, data were obtained from TCGA Firehose Legacy dataset for COADREAD (illumina_hiseq_rnaseqv2-RSEM_genes_normalized) at <https://gdac.broadinstitute.org/>. Colorectal cancer tumors were identified from the dataset for stage of disease progression and KRAS mutation status from <https://www.cbiportal.org/>.

Proliferation Assay by Cell Counting

To measure cellular proliferation and cell death, manual cell counting assays were performed. On day -5, cells were split and treated with either DMSO or tazemetostat. On day -3, cells were passaged 1:2 and maintained in DMSO or tazemetostat. On day -1, cells were seeded in triplicate in six-well plates (100,000–150,000 cells/well) for counting for day 0 timepoint and day 5 timepoint (unless otherwise stated) and 10 cm plates for protein lysates. For cell counting assays including siRNAs, cells were transfected with siRNA on day -1 and incubated for at least 8 hours before seeding. Twenty-four hours after seeding, a day 0 count was taken. Cells were trypsinized, spun down, resuspended in PBS, and manually counted in a hemocytometer. Experimental plates were dosed with the indicated compounds by replacing the media. On day 1, protein lysates were collected 16 to 24 hours after dosing, unless otherwise stated. For counting plates, the media and drug were refreshed after 3 days. During a final day 5 timepoint, the cells were counted using a hemocytometer. Final counts were normalized

to respective day 0 counts, and log₂ fold change and percent change were calculated for graphical representation. Data points represent technical replicates from a representative experiment. All counting experiments and associated Western blots were repeated at least three times independently.

Incucyte Live Cell Imaging

Similar to cell counting assays, after cells were pretreated for 5 days with tazemetostat or DMSO, the cells were seeded at 3,000 to 6,000 cells per well in 96-well clear-bottom black plates (Thermo Fisher Scientific, #165305) at three to five technical replicates per treatment condition with four images taken per technical replicate. Nuclei were either labeled by stably expressing Incucyte Nuclight Red (Sartorius, #4625) or transiently labeled with Incucyte Nuclight Rapid Red Reagent (Sartorius, #4717). Twenty-four hours after seeding, the cells were treated with media containing the indicated drug and CellEvent Caspase-3/7 Green Detection Reagent (Invitrogen, #C10423) at a final 1:1,000 dilution to detect the presence of caspase activity and apoptosis. Four images were acquired at 10× magnification in phase, green (300 ms acquisition time), and red (400 ms acquisition time) channels every 2 hours. Image acquisition and analysis were conducted using Incucyte S3 software. To determine the number of caspase 3/7-positive cells, the overlap (green and red) counts per well were normalized to red counts/well at each timepoint.

Synergy Analysis

CellTiter-Glo assays were conducted to determine the synergistic interactions between EZH2 inhibitors (0, 1, 2.5, and 5 μmol/L) and MEK inhibitors (0, 1, 5, 10, and 50 nmol/L). Cells were seeded at 3,000 to 6,000 cells per well in a 96-well white flat-bottom plates with three technical replicates per treatment condition. Twenty-four hours after seeding, the cells were dosed with varying indicated concentrations of EZH2 and MEK inhibitors. Five days after combined treatment, cell viability was measured using CellTiter-Glo (Promega, #G9291), normalized to a day 0 measurement and then to DMSO to calculate the inhibitory response. Synergy scores were calculated using the Gaddum's non-interaction model—HSA with SynergyFinder (60). An HSA value greater than 10 indicates a synergistic interaction.

Western Blot

Cell lysates were harvested after 16 to 24 hours after vehicle or drug treatment. Cells were washed with PBS, lysed in boiling 1% SDS lysis buffer [1% SDS (Invitrogen, #15553-035), 10 mmol/L Tris-HCl pH 7.5 (Sigma, #77-86-1), and 100 mmol/L NaCl (Sigma, #S5586)], scraped, collected, boiled at 95°C for 10 to 15 minutes, and spun down at maximum speed for 3 minutes. Protein concentration was determined using bicinchoninic acid quantification (Bio-Rad, #23222). Proteins were run on SDS-PAGE gels (Bio-Rad, #4561084) and transferred to Immobilon nitrocellulose membranes (Bio-Rad, #1620115). The membranes were blocked in 5% milk in Tris-buffered saline with Tween 20 (TBST) for 30 to 60 minutes and then incubated with primary antibodies overnight at 4°C. Membranes were incubated with infrared dye-conjugated (IRDye 800CW, #926-32213; IRDye 680CW, #926-68072) or HRP-conjugated secondary antibodies for 1 hour, and signal was measured using Odyssey LICOR Fc or autoradiographic film. The following antibodies were used at 1:500 to 1:1,000 dilution unless otherwise stated: pERK (CST, #4370, RRID: AB_2315112), ERK (CST, #9102, RRID:AB_330744), H3K27me3 (CST, #9733, RRID:AB_2616029), Histone H3 (CST, #4499, RRID:AB_10544537), TLE4 (Abcam, #ab64833, RRID:AB_2203850), HA-tag (CST, #3724, RRID:AB_1549585), ATOH1 (Proteintech, #21215-1-AP, RRID: AB_10733126), LGR5 (Abcam, #75850, RRID:AB_1523716), SOX9 (EMD Millipore, #AB5535 1:5,000, RRID:AB_2239761), PROM1 (CST, #64326, RRID:AB_2721172), CDX2 (CST, #12306, RRID:

AB_2797879), KRT20 (CST, #13063, RRID:AB_2798106), KLF4 (CST, #4038, RRID:AB_2265207), CDCA7 (Proteintech, #15249-1-AP, RRID:AB_2878119), GAPDH (CST, #2118, RRID:AB_561053), vinculin (Santa Cruz Biotechnology, #sc-25336, RRID:AB_628438), β-catenin (CST, #8814, RRID:AB_11127203), p-RB (CST, #9308, RRID:AB_331472), RB (CST, #9313S, RRID:AB_1904119), p21 (CST, #2947, RRID:AB_823586), and p27 (SantaCruz, #sc-528, RRID:AB_632129).

RNA Extraction and Quantitative PCR

Total RNA was isolated after 16 to 24 hours of vehicle, single-agent, or combination treatment using the RNeasy Plus Mini kit (Qiagen, #74136) and reverse transcribed to cDNA using the qScript cDNA synthesis kit (Quantabio, #95047-500) following the manufacturer's instructions. qPCR amplification was done using PerfeCTa SYBR Green SuperMix Reagent (Quantabio, #95054-500), and reactions were run on the Bio-Rad CFX96 cyler in technical triplicates. Relative expression was calculated by first normalizing to housekeeping genes *STAU1* or *UBC* and then to the DMSO sample using the ΔΔCq method.

Transfections and Infections

For siRNA experiments, cells were incubated for 6 to 8 hours with 0.1 μmol/L siRNA constructs with a 1:400 dilution of Lipofectamine RNAiMAX transfection reagent (Invitrogen, #13778075) in antibiotic-free media. Non-targeting *BMF*, *TLE4*, *CDX2*, *TRPS1*, *SOX6*, *ATOH1*, *MAF*, *DACH1*, *PTPRD*, *TSHZ2*, *CSMD1*, *EYA4*, *SMOC2*, *ATOH8*, *WNT5A*, *PPARGC1A*, *DEFA5*, *CADM1*, *CELF2*, *GLI3*, *CTNBN1* ON-TARGETplus pools and non-target controls were purchased from Horizon Biosciences (catalog #: D-001810-10, L-004393-00, L-019336-00, L-015636-00, L-009644-00, L-015101-01, L-008915-01, L-003746-00, L-013222-00, L-008527-00, L-018447-02, L-007288-00, L-011853-00, L-013886-02, L-008817-00, L-003939-00, L-005111-00, L-013143-01, L-016565-00, L-012741-00, L-011043-00, and L-003482-00, respectively).

Oligos

Oligos used for primers for RT-qPCR are listed as follows in 5'-3' orientation: *BMF* (fwd: ACTTCAGCTCTCCCTCTCA, rev: GAGTCTGGGTAGCTTTGTCTTC), *UBC* (fwd: ATTTGGGTCG CGGTTCTT, rev: TGCCTTGACATTCTCGATGGT), *STAU1* (fwd: GGATGAGTTCAGGATGCCTTAT, rev: GGTGTGATGTCCTTG ACTAACT), *MAF* (fwd: TGGAGTCGGAGAAGAACCA, rev: CTG CTCACCAACTTCTCGTATT), *DACH1* (fwd: GGAAGGGTGGCT ATGTGTTATT, rev: GCACTGTTTGCCGCTTTAC), *PTPRD* (fwd: CTGTGAGAGGAGCAACGAATA, rev: GTGCAGCCAGACGGAA ATA), *TSHZ2* (fwd: CCAGACATCAGAGGGCAAATAC, rev: GGTC ATTGAGAGTCCCGTAAAC), *CSMD1* (fwd: AACCCTACCTTCG TGCATAG, rev: GTTGTGCATACGGAGCTGGATAG), *EYA4* (fwd: ATCTCTCCCAGGACTGACTAAC, rev: ACTCCTACAGGTTCT CTCATCAA), *SMOC2* (fwd: GACCTTCCTTCCCGTTGT, rev: GCTCCTGGGTATACTTCCCTTC), *ATOH8* (fwd: GGCAGAAGC TGTCCAACT, rev: ACTGTAGTCAAGGTCAGCCA), *WNT5A* (fwd: CCTAGTGGCTTTGGCCATATT, rev: TCTGACATCTGAACAGGG TTATT), *PPARGC1A* (fwd: TGAAGTGGGACAGTGATTTC, rev: CCCAAGGGTAGTCTAGTTTATC), *DEFA5* (fwd: CCATCCTTGC TGCCATTCT, rev: GTTGTAGCTTCATCAGCTCTTT), *CADM1* (fwd: GCTTCTGCTGTTGCTCTTCT, rev: CTCGACTACTGTCA CGTCTTTC), *CELF2* (fwd: GAACCTCCGACAGAGTAAAG, rev: GGATGATGCATCCAGGTAAG), *TLE4* (fwd: CAGCCTGCTCAA CCCTTTA, rev: CCAGCTCAGACTGTGGTATT), and *GLI3* (fwd: TCTGACCGATGGAGGTAGTATAG, rev: GTTGCAGTGGAAATGG TTGAG). Oligos used for sgRNAs for CRISPR are listed as follows in 5'-3' orientation: *BMF* (fwd: GGGAGCCGGTGACCAACCC, rev:

GGGTTGGGTACCCGGCTCCC), *TLE4* #1 (fwd: CCGGCACTGCTACCGATGGG, rev: CCCATCGGTAGCAGTGCCGG), and *TLE4* #2 (fwd: CATGACAATGATACCAAAG, rev: CTTTGGTGATCATGTCATG).

For CRISPR knockouts, oligos were purchased from Invitrogen with the described sequences and cloned into CRISPR Lenti-v2 backbone. For ectopic constitutive β -catenin expression, the pLV β -catenin $\Delta 90$ construct and its corresponding empty vector control were purchased from Addgene (#36985 and #85139). For ectopic *SOX9* expression, the pLX304 *SOX9* construct was a gift from Dr. Nilay Sethi from Dana-Farber. For ectopic *TLE4* expression, the pLX304 *TLE4* construct was purchased from Horizon Biosciences (Cat #OHS6085-213583570) from the CCSSB-Broad Lentiviral Expression Collection. Lentivirus was produced in 293T cells using X-tremeGENE 9 DNA Transfection Reagent (Roche, #6365787001) and collected 72 hours after transfection. Cells were infected twice for 24 hours each at 1:2 dilution in the presence of 8 μ g/mL polybrene. Cells were recovered from the infection for 24 hours and selected in 2 μ g/mL puromycin for 3 to 5 days.

HA-BMF Knockin

An N-terminal HA-tag was introduced into the endogenous locus of *BMF* as previously described (57). The crRNA (5'-TTGCCCCCTCACAGGAGAGA-3') was hybridized with Alt-R CRISPR-Cas9 tracrRNA (IDT, #1073190) at 95°C for 5 minutes at an equimolar ratio (0.375 nmol). The mix was cooled down to room temperature on the benchtop for 10 minutes before adding 2 μ L of Alt-R S.p.Cas9 Nuclease V3 (IDT, #1081059) and 5 μ L of 100 μ mol/L single-stranded donor oligonucleotide (5'-GCTGAGGGGGCAGTCCAGTAGGCTCTGGGCAACAGGTCAGCAGAGAGCAAGCTCCCAGGTTGGGTCACCCGGTCCCCATCCTCTGGTTGGAACACATCCTCTCCAGTCTCCACACACTGAGATGGCTCAGCGTAATCTGGTACGTCGTATGGGTACATCTCCTCTGGAGGGGCAACGCAGGCATCTGGGCTGCT-3'). The mix was incubated for 20 minutes at room temperature and added to 1 million LOVO and SW620 cells resuspended in 100 μ L of SF Cell Line Nucleofector solution (Lonza, V4XC-2012). Cells were then transferred to a cuvette and nucleofected using the E0-117 program in a 4D-Nucleofector X Unit (Lonza).

RNA-seq

Total RNA was isolated after 16 to 24 hours of vehicle, single-agent, or combination treatment using the RNeasy Plus Mini kit (Qiagen, #74136). RNA was sequenced at the Dana-Farber Cancer Institute Molecular Biology Core Facility using the Illumina NextSeq 500 system, or with Novogene UC Davis Sequencing Center. Raw data were mapped to the hg38 genome using STAR (RRID:SCR_004463), and count files were generated using HTSeq (RRID:SCR_005514). DESeq2 (RRID:SCR_015687) was used to normalize gene counts (the mean ratio method) and determine differentially expressed genes. Differentially expressed genes between different treatment conditions (combo vs. DMSO, combo vs. EZH2i) were defined as \log_2 fold change >1 and Benjamini-Hochberg corrected *P* value < 0.05.

ssGSEA and GSEA

ssGSEA was performed using GenePattern (<http://genepattern.org/>) using the normalized gene counts matrix. GSEA was performed using GSEA_4.2.3 software (RRID:SCR_003199) from <http://gsea-msigdb.org/>. Gene signatures from GO:BP were obtained from Molecular Signatures Database (RRID:SCR_016863; <https://www.gsea-msigdb.org/gsea/msigdb>). GO analysis was performed with differentially upregulated PRC2 targets using DAVID (RRID:SCR_001881; <https://david.ncifcrf.gov/>).

CUT&RUN, Illumina Sequencing, and Data Analysis

CUT&RUN was performed as previously described (61). In brief, 500,000 nuclei from LOVO cells treated with DMSO, 50 nmol/L trametinib, 5 μ mol/L tazemetostat, or the combination of both drugs were isolated using nuclear extraction buffer (20 mmol/L HEPES pH 7.9, 10 mmol/L KCl, 0.1% Triton X-100, 20% glycerol, and 1 mmol/L MnCl₂). Nuclei samples were then immobilized to BioMag Plus Concanavalin A (ConA)-coated magnetic beads (Bangs Laboratories, #BP531) that were activated by washing three times with cold bead activation buffer (20 mmol/L HEPES pH 7.9, 10 mmol/L KCl, 1 mmol/L CaCl₂, and 1 mmol/L MnCl₂). ConA bead/cell mixtures were resuspended in cold antibody buffer (20 mmol/L HEPES pH 7.5, 150 mmol/L NaCl, 0.5 mmol/L spermidine, 1 \times Roche cOmplete, Mini, EDTA-free protease inhibitor, 0.01% digitonin, and 2 mmol/L EDTA), then incubated with 0.5 μ g primary antibodies [H3K27me3 (CST, #9733, RRID:AB_2616029) and H3K4me3 (CST, #9751, RRID:AB_2616028) or IgG (Epicpypher, #13-0042, RRID:AB_2923178)] overnight at 4°C in the cold room. Unbound antibodies were washed three times each with cold digitonin buffer (20 mmol/L HEPES pH 7.5, 150 mmol/L NaCl, 0.5 mmol/L spermidine, 1 \times Roche cOmplete, Mini, EDTA-free protease inhibitor, and 0.01% digitonin). ConA bead/cell mixtures were then resuspended in 50 μ L cold digitonin buffer and incubated with our homemade pAG-MNase at 4°C in the cold room for an hour on a nutator. Unbound pAG-MNase was washed three times with cold digitonin buffer. MNase was activated by the addition of CaCl₂ and incubated at 4°C in the cold room for 30 minutes on a nutator to cleave and release antibody-bound chromatin. The reaction was stopped by adding cold stop buffer (340 mmol/L NaCl, 20 mmol/L ethylene glycol-bis(2-aminoethylether)-N,N,N',N'-tetraacetic acid, egtazic acid (EDTA), 4 mmol/L EGTA, 50 μ g/mL RNase A, 50 μ g/mL glycogen, and 1 pg/ μ L *E. coli* spike-in DNA). Released chromatin was then released by incubating at 37°C for 10 minutes. CUT&RUN enriched DNA in the supernatant can be collected using magnetic beads and purified using the Monarch PCR and DNA clean-up kit (NEB, #T1030L). CUT&RUN libraries were prepared with 10 ng CUT&RUN DNA using the NEBNext Ultra II DNA Library Prep Kit (NEB, #E7645), according to the manufacturer's protocol. Libraries were sequenced on Illumina NextSeq2000, 2 \times 50-bp paired-end reads.

Paired-end fastq files were aligned to hg38 reference genome using Bowtie2 (RRID:SCR_016368) with the setting “-very-sensitive -no-mixed -no-discordant -phred33 -I 10 -X 700”. Sequencing reads were also aligned to the *E. coli* genome to map spike-in reads. For spike-in normalization, the total number of mapped reads to the *E. coli* genome was used to calculate the normalization factor for CUT&RUN samples. SAM files were converted to bam files using Samtools (RRID:SCR_002105). Bigwig files were generated from bam files using Deeptools with “scale-factor” option of bamCoverage for spike-in normalization (RRID:SCR_016366). Genome browser tracks of big files were generated using Integrative Genomics Viewer (IGV) (RRID:SCR_011793). Peaks were called using MACS2 (RRID:SCR_013291) using the callpeak function with “-f BAME -keep-dup 1 -q 0.05” and IgG was used as controls. DESeq2 analysis from DiffBind R package with option “spikein = True” was used to compare differential binding between conditions (FDR < 0.1).

In Vivo Xenograft Assays

For the PDX tumors, the tissue specimens to establish the colorectal cancer PDX models were collected in accordance with the Dana-Farber/Harvard Cancer Center Institutional Review Board protocol 03-189, where model generation and sharing of deidentified samples are covered under the consent. Six- to eight-week-old athymic Nu/Nu mice were purchased from Charles River Laboratory. LOVO xenografts were generated by injecting 3 million cells in PBS subcutaneously in the rear flanks of nude mice. For the PDX models,

tumors were passed from seed mice, cut into 2 × 2 × 2-mm chunks, and implanted subcutaneously in the rear flank of nude mice. For the LOVO cell line xenograft, two tumors per mouse were used. For the human PDX models, COCA9, COCA74P, COCA4, and COCA30, one tumor per mouse was used. When tumors reached 50 to 150 mm³, mice were randomized and enrolled into either vehicle or tazemetostat pretreatment arms. At least 5 to 10 tumors were used per treatment arm to detect a 50% change in tumor volume between the combo treatment arms and the single-agent arms with a power of at least 80% and FDR of 5%.

In Vivo Drug Treatments

Mice were pretreated for 7 days and then randomized and enrolled into treatment arms: vehicle (tazemetostat vehicle with trametinib vehicle), trametinib (trametinib with tazemetostat vehicle), tazemetostat (tazemetostat with trametinib vehicle), or combination (tazemetostat with trametinib). Tazemetostat was prepared in 0.5% methylcellulose (FUJIFILM Wako Chemicals, #13317815) containing 0.1% Tween-80 and dosed at 250 mg/kg twice a day via oral gavage. Trametinib was prepared in 0.5% hydroxypropyl methylcellulose (Sigma, #H7509) containing 0.2% Tween-80, pH 8.0, and dosed at 0.6 mg/kg once a day via oral gavage. Tumor volume was measured using Vernier calipers two to three times a week and calculated with the formula (width × length² × 0.52).

Organoids

Organoid lines were derived and cultured as previously described (33, 62). In brief, isolated crypts were resuspended in Matrigel (Corning, #356231), plated in six-well plates, and overlaid with growth medium comprising advanced DMEM/F12 (#12634010) supplemented with penicillin-streptomycin (#15070063); 10 mmol/L HEPES (#15630080); 2 mmol/L GlutaMAX (#35050061), N2 (#17502048), and B27 (#17504044; all from Gibco, Life Technologies); 100 ng/mL Noggin (PeproTech #250-38); and EGF (PeproTech #AF-100-15). As tumor organoid lines harbor *Apc* mutations, R-spondin and WNT3A were not supplemented. Organoids were dissociated into single cells with TrypLE Express (Gibco, #12604021) and seeded in 50 to 100 cells per μ L of Matrigel. For counting experiments, organoids were seeded in 7 × 20 μ L domes of Matrigel per well of a six-well plate. Cells were cultured in DMSO or 5 μ mol/L of tazemetostat for 2 days, seeded into experimental plates with continued pretreatment of DMSO and tazemetostat, and allowed to form spheres for an additional 3 to 5 days before the addition of 50 nmol/L of trametinib. On days 0 and 3 after combination treatment, organoids were dissociated into single cells with TrypLE Express, spun down, resuspended in PBS, and manually counted in a hemocytometer. Final counts were normalized to respective day 0 counts, and log₂ fold change was calculated for graphical representation.

Human Patient-Derived Organoids

Human patient-derived organoids were cultured as described (63). In brief, human organoids were cultured in organoid growth media as described above, with the addition of N-acetylcysteine (NAC) (#A9165), nicotinamide (#N3376), SB202190 (#S7067), A83 (#SML0788), prostaglandin E (#P5640; all from Sigma Aldrich); WNT3A (R&D Systems, #5036-WN); R-spondin (PeproTech, #120-38); and FBS. Patient-derived organoids were dissociated into single cells, and 5,000 cells were seeded in 30 μ L of Matrigel in a 96-well plate. Cells were cultured in DMSO or 5 μ mol/L of tazemetostat for 5 days and then treated on day 0 with DMSO or trametinib for an additional 5 days. Cell number was indirectly assessed using the CellTiter-Glo 3D Viability Assay (Promega, #G9683) according to the manufacturer's instructions on day 0 prior to the addition of trametinib and on day 5 after combination treatment.

Tissue-Based CyCIF

Formalin-fixed, paraffin-embedded sections of mouse colons, CDX, and PDX samples were stained with a 15-plex antibody panel. High-plex images were acquired using the CyCIF technique (64). In brief, slides first underwent dewaxing and antigen retrieval using a preset protocol on the Leica BOND RX. Sections were then bleached with 4.5% H₂O₂ and 25 mmol/L NaOH in 1× PBS under LED light for 1 hour at room temperature. Subsequently, the slides were blocked overnight at 4°C in darkness with secondary antibodies (1:1,000 dilution) in SuperBlock blocking buffer (Thermo Fisher Scientific, #37515) to reduce autofluorescence and nonspecific secondary background. In each staining cycle, samples were incubated overnight at 4°C in darkness with Hoechst 33342 (1:10,000; Thermo Fisher Scientific, cat. # 62249) for nuclear staining and appropriate antibodies diluted in SuperBlock blocking buffer. Post-staining, the slides were washed and mounted/cover slipped with 50% glycerol/PBS for imaging on CyteFinder II HT (RareCyte), using a 20× 0.75NA objective. Between cycles, fluorophores were photobleached with the H₂O₂ solution as described earlier, and the slides were washed thoroughly before incubating antibodies for the next cycle. The multiplexed whole-slide images were processed via the Docker-based NextFlow pipeline, MCMICRO (65). Essentially, the raw images underwent stitching, registration, segmentation, and single-cell quantification of fluorescence intensities. The full codebase is available on GitHub (<https://github.com/labsyspharm/mcmicro>). Antibodies used were SOX9 (Abcam, #ab202516, 1:200, RRID:AB_2943105), KRT20 (CST, #63126, 1:200, RRID: AB_3101888), pERK (CST, #4344S, 1:200, RRID:AB_2139960), CDX2 (Abcam, #ab195008, 1:400, RRID:AB_2889213), panCK (eBioscience, #53-9003-82, 1:800, RRID:AB_1834350), and SMA (Invitrogen, #41-9760-82, 1:800, RRID:AB_2573631).

Analysis of PRC2 Target Genes

To identify relevant PRC2 targets, we analyzed genes that had differentially lost H3K27me3 binding between combo and DMSO-treated LOVO cells from the CUT&RUN data (adjusted *P* value < 0.05, FDR < 0.05, fold change < -1, and nearest distance to transcription start site annotation < 5 kb). We overlapped these genes with those that were differentially upregulated between combo and DMSO-treated LOVO cells from the RNA-seq data (adjusted *P* value < 0.05, fold change > 1, and base mean expression > 10).

Generation of a Curated β -Catenin-Regulated Signature

β -Catenin-regulated signature is a generated set of 175 genes identified from RNA-seq experiments that were simultaneously downregulated by EZH2 and MEK inhibitors versus DMSO (log₂ fold change < -1) and upregulated or rescued in β -catenin Δ 90 combo versus empty vector combo (log₂ fold change > 0.5). This signature represents β -catenin-regulated targets that are critical for the cytotoxic effects of EZH2 and MEK inhibitors in colorectal cancer cell lines.

Quantification and Statistical Analysis

For quantitative measurements *in vitro*, graphs depict the mean of the indicated number of technical replicates \pm SD, unless otherwise noted. The *in vivo* tumor volume over time graphs represent the mean \pm SEM. Statistical tests, including two-tailed unpaired *t* tests, ANOVA followed by Tukey multiple comparisons test, Mann-Whitney tests, or log-rank tests were used to compare experiment groups, and *P* values are indicated. A *P* value less than 0.05 was considered significant. All data were graphed and analyzed using GraphPad Prism v9.2.0 (RRID:SCR_002798).

Ethics Reporting

All mouse work was done in compliance with the Institutional Animal Care and Use Committee at Brigham and Women's Hospital and Animal Welfare Act (Approved Protocol #2016N000467). Written informed consent was obtained from patients for the use of their tumor specimens and clinical and genomic data. The study was conducted in accordance with recognized ethical guidelines (e.g., Declaration of Helsinki, CIOMS, Belmont Report, U.S. Common Rule) and was approved by the Dana-Farber/Harvard Cancer Center Institutional Review Board.

Data Availability

RNA-seq data for LOVO, SW620, SK-CO1, and LS513 cells treated with EZH2, MEK, and KRAS inhibitors are available under GEO database GSE265926. RNA-seq data for LOVO cells expressing empty vector or β -catenin Δ 90 treated with EZH2 and MEK inhibitors are available under GEO database GSE265906. LOVO cells transduced with sgControl or sgTLE4 and treated with EZH2 and MEK inhibitors are available under GEO database GSE265907. H3K27me3 CUT&RUN data are available under BioProject PRJNA1104573.

Authors' Disclosures

P. Loi reports grants from the NIH/NCI during the conduct of the study. A.E. Schade reports grants from the American Cancer Society during the conduct of the study. M. Watanabe reports grants from Brigham and Women's Hospital during the conduct of the study. O. Popow reports grants from Cancer Research UK and the Mark Foundation for Cancer Research during the conduct of the study. N. Gunduz reports grants from Cancer Grand Challenges during the conduct of the study. M. Giannakis reports grants from Janssen and personal fees from Nerviano Medical Sciences outside the submitted work. K. Ng reports nonfinancial support from Pharmavite, grants from Janssen, personal fees from Bayer, GlaxoSmithKline, Pfizer, CytomX, Jazz Pharmaceuticals, Revolution Medicines, AbbVie, Etiome, Seagen, CRICO, and JAMA outside the submitted work. S. Santagata reports being speaker honoraria for Novartis and Roche. K. Helin reports grants from the Cancer Research UK Grand Challenge and the Mark Foundation for Cancer Research to the SPECIFICANCER team during the conduct of the study. O.J. Sansom reports grants from AstraZeneca, Novartis, Boehringer Ingelheim, and Cancer Research Horizons outside the submitted work. K. Cichowski reports grants from Cancer Research UK and the Mark Foundation for Cancer Research during the conduct of the study, as well as other support from Erasca outside the submitted work. No disclosures were reported by the other authors.

Authors' Contributions

P. Loi: Conceptualization, resources, data curation, formal analysis, methodology, writing—original draft, writing—review and editing, design. **A.E. Schade:** Conceptualization, resources, data curation, formal analysis, methodology, writing—original draft, writing—review and editing, design. **C.L. Rodriguez:** Resources, data curation, project administration. **A. Krishnan:** Resources, data curation, project administration. **N. Perurena:** Resources, data curation. **V.T.M. Nguyen:** Resources, data curation, formal analysis. **Y. Xu:** Resources, data curation, formal analysis. **M. Watanabe:** Resources, data curation. **R.A. Davis:** Resources, data curation. **A. Gardner:** Resources, data curation. **N.F. Pilla:** Resources, data curation. **K. Mattioli:** Formal analysis. **O. Popow:** Resources, data curation. **N. Gunduz:** Resources, data curation. **T.R.M. Lannagan:** Resources, data curation, project administration. **S. Fitzgerald:** Resources, data curation, project administration. **E.T. Sicinska:** Resources, data curation, project administration. **J.-R. Lin:** Resources, data curation, formal

analysis. **W. Tan:** Project administration. **L.K. Brais:** Project administration. **K.M. Haigis:** Resources, data curation. **M. Giannakis:** Resources, data curation, writing—original draft, writing—review and editing. **K. Ng:** Resources, data curation. **S. Santagata:** Resources, data curation, supervision. **K. Helin:** Resources, data curation. **O.J. Sansom:** Resources, data curation, supervision. **K. Cichowski:** Conceptualization, resources, data curation, supervision, methodology, writing—original draft, writing—review and editing, design.

Acknowledgments

This work was supported by a grant from the Cancer Research UK Grand Challenge and the Mark Foundation for Cancer Research to the SPECIFICANCER team (K. Cichowski, K.M. Haigis, O.J. Sansom, and K. Helin). P. Loi was supported by the NIH/NCI Ruth Kirschstein National Research Service Award (F31CA260804). A.E. Schade was supported by an American Cancer Society—Cancer Research Racquet and Women's Tennis Association—Postdoctoral Fellowship, PF-22-040-01-ET. A. Gardner was supported by a NIH/NCI Predoctoral to Postdoctoral Fellow Transition Award (K00CA245807).

Note

Supplementary data for this article are available at Cancer Discovery Online (<http://cancerdiscovery.aacrjournals.org/>).

Received August 4, 2023; revised June 19, 2024; accepted August 7, 2024; published first August 12, 2024.

REFERENCES

- Kuipers EJ, Grady WM, Lieberman D, Seufferlein T, Sung JJ, Boelens PG, et al. Colorectal cancer. *Nat Rev Dis Primers* 2015;1:15065.
- O'Connell JB, Maggard MB, Ko CY. Colon cancer survival rates with the new American joint committee on cancer sixth edition staging. *J Natl Cancer Inst* 2004;96:1420–5.
- Brenner H, Kloor M, Pox CP. Colorectal cancer. *Lancet* 2014;383:1490–502.
- Morel D, Jeffery D, Aspeslagh S, Almouzni G, Postel-Vinay S. Combining epigenetic drugs with other therapies for solid tumours—past lessons and future promise. *Nat Rev Clin Oncol* 2020;17:91–107.
- Ryan MB, Corcoran RB. Therapeutic strategies to target RAS-mutant cancers. *Nat Rev Clin Oncol* 2018;15:709–20.
- Serebriiskii IG, Connelly C, Frampton G, Newberg J, Cooke M, Miller V, et al. Comprehensive characterization of RAS mutations in colon and rectal cancers in old and young patients. *Nat Commun* 2019;10:3722.
- Fearon ER, Vogelstein B. A genetic model for colorectal tumorigenesis. *Cell* 1990;61:759–67.
- Amado RG, Wolf M, Peeters M, Van Cutsem E, Siena S, Freeman DJ, et al. Wild-type KRAS is required for panitumumab efficacy in patients with metastatic colorectal cancer. *J Clin Oncol* 2008;26:1626–34.
- Knickerlein K, Zhang L. Mutant KRAS as a critical determinant of the therapeutic response of colorectal cancer. *Genes Dis* 2015;2:4–12.
- Yaeger R, Weiss J, Pelster MS, Spira AI, Barve M, Ou S-HI, et al. Adagrasib with or without cetuximab in colorectal cancer with mutated KRAS G12C. *N Engl J Med* 2023;388:44–54.
- Ji J, Wang C, Fakhri M. Targeting KRAS^{G12C}-mutated advanced colorectal cancer: research and clinical developments. *Onco Targets Ther* 2022;15:747–56.
- de Sousa E Melo F, de Sauvage FJ. Cellular plasticity in intestinal homeostasis and disease. *Cell Stem Cell* 2019;24:54–64.
- Jadhav U, Saxena M, O'Neill NK, Saadatpour A, Yuan G-C, Herbert Z, et al. Dynamic reorganization of chromatin accessibility signatures during dedifferentiation of secretory precursors into Lgr5+ intestinal stem cells. *Cell Stem Cell* 2017;21:65–77.e5.
- Hanahan D. Hallmarks of cancer: new dimensions. *Cancer Discov* 2022;12:31–46.

15. Margueron R, Reinberg D. The Polycomb complex PRC2 and its mark in life. *Nature* 2011;469:343–9.
16. Golbabapour S, Majid NA, Hassandarvish P, Hajrezaie M, Abdulla MA, Hadi AHA. Gene silencing and Polycomb group proteins: an overview of their structure, mechanisms and phylogenetics. *OMICS* 2013;17:283–96.
17. Bracken AP, Dietrich N, Pasini D, Hansen KH, Helin K. Genome-wide mapping of Polycomb target genes unravels their roles in cell fate transitions. *Genes Dev* 2006;20:1123–36.
18. Schuettengruber B, Bourbon H-M, Di Croce L, Cavalli G. Genome regulation by Polycomb and Trithorax: 70 years and counting. *Cell* 2017;171:34–57.
19. Bracken AP, Helin K. Polycomb group proteins: navigators of lineage pathways led astray in cancer. *Nat Rev Cancer* 2009;9:773–84.
20. Wassef M, Margueron R. The multiple facets of PRC2 alterations in cancers. *J Mol Biol* 2017;429:1978–93.
21. Comet I, Riising EM, Leblanc B, Helin K. Maintaining cell identity: PRC2-mediated regulation of transcription and cancer. *Nat Rev Cancer* 2016;16:803–810.
22. Varambally S, Dhanasekaran SM, Zhou M, Barrette TR, Kumar-Sinha C, Sanda MG, et al. The polycomb group protein EZH2 is involved in progression of prostate cancer. *Nature* 2002;419:624–629.
23. Kleer CG, Cao Q, Varambally S, Shen R, Ota I, Tomlins SA, et al. EZH2 is a marker of aggressive breast cancer and promotes neoplastic transformation of breast epithelial cells. *Proc Natl Acad Sci U S A* 2003;100:11606–11.
24. Zingg D, Debbache J, Peña-Hernández R, Antunes AT, Schaefer SM, Cheng PF, et al. EZH2-mediated primary cilium deconstruction drives metastatic melanoma formation. *Cancer Cell* 2018;34:69–84.e14.
25. Morin RD, Johnson NA, Severson TM, Mungall AJ, An J, Goya R, et al. Somatic mutations altering EZH2 (Tyr641) in follicular and diffuse large B-cell lymphomas of germinal-center origin. *Nat Genet* 2010;42:181–5.
26. Koppens MA, Bounova G, Gargiulo G, Tanger E, Janssen H, Cornelissen-Steijger P, et al. Deletion of polycomb repressive complex 2 from mouse intestine causes loss of stem cells. *Gastroenterology* 2016;151:684–97.e12.
27. Knutson SK, Warholc NM, Wigle TJ, Klaus CR, Allain CJ, Raimondi A, et al. Durable tumor regression in genetically altered malignant rhabdoid tumors by inhibition of methyltransferase EZH2. *Proc Natl Acad Sci U S A* 2013;110:7922–7.
28. Cook JH, Melloni GEM, Gulhan DC, Park PJ, Haigis KM. The origins and genetic interactions of KRAS mutations are allele- and tissue-specific. *Nat Commun* 2021;12:1808.
29. Hallin J, Bowcut V, Calinisan A, Briere DM, Hargis L, Engstrom LD, et al. Anti-tumor efficacy of a potent and selective non-covalent KRAS^{G12P} inhibitor. *Nat Med* 2022;28:2171–82.
30. Kopetz S, Grothey A, Yaeger R, Van Cutsem E, Desai J, Yoshino T, et al. Encorafenib, binimetinib, and cetuximab in BRAF V600E-mutated colorectal cancer. *N Engl J Med* 2019;381:1632–43.
31. Bholra PD, Ahmed E, Guerriero JL, Sicinska E, Su E, Lavrova E, et al. High-throughput dynamic BH3 profiling may quickly and accurately predict effective therapies in solid tumors. *Sci Signal* 2020;13:eaay1451.
32. Hinze L, Labrosse R, Degar J, Han T, Schatoff EM, Schreek S, et al. Exploiting the therapeutic interaction of WNT pathway activation and asparaginase for colorectal cancer therapy. *Cancer Discov* 2020;10:1690–705.
33. Fumagalli A, Drost J, Suijkerbuijk SJE, van Boxtel R, de Ligt J, Offerhaus GJ, et al. Genetic dissection of colorectal cancer progression by orthotopic transplantation of engineered cancer organoids. *Proc Natl Acad Sci U S A* 2017;114:E2357–64.
34. Jackstadt R, van Hooff SR, Leach JD, Cortes-Lavaud X, Lohuis JO, Ridgway RA, et al. Epithelial NOTCH signaling rewires the tumor microenvironment of colorectal cancer to drive poor-prognosis subtypes and metastasis. *Cancer Cell* 2019;36:319–36.e7.
35. Merenda A, Fenderico N, Maurice MM. Wnt signaling in 3D: recent advances in the applications of intestinal organoids. *Trends Cell Biol* 2020;30:60–73.
36. Gu W, Wang H, Huang X, Krawczyk J, Singh PNP, Ng C, et al. SATB2 preserves colon stem cell identity and mediates ileum-colon conversion via enhancer remodeling. *Cell Stem Cell* 2022;29:101–15.e10.
37. Haber AL, Biton M, Rogel N, Herbst RH, Shekhar K, Smillie C, et al. A single-cell survey of the small intestinal epithelium. *Nature* 2017;551:333–9.
38. Kim T-H, Li F, Ferreira-Neira I, Ho L-L, Luyten A, Nalapareddy K, et al. Broadly permissive intestinal chromatin underlies lateral inhibition and cell plasticity. *Nature* 2014;506:511–5.
39. Sphyris N, Hodder MC, Sansom OJ. Subversion of niche-signalling pathways in colorectal cancer: what makes and breaks the intestinal stem cell. *Cancers (Basel)* 2021;13:1000.
40. Fevr T, Robine S, Louvard D, Huelsken J. Wnt/ β -catenin is essential for intestinal homeostasis and maintenance of intestinal stem cells. *Mol Cell Biol* 2007;27:7551–9.
41. Pinto D, Gregorieff A, Begthel H, Clevers H. Canonical Wnt signals are essential for homeostasis of the intestinal epithelium. *Genes Dev* 2003;17:1709–13.
42. Dow LE, O'Rourke KP, Simon J, Tschaharganeh DF, van Es JH, Clevers H, et al. Apc restoration promotes cellular differentiation and reestablishes crypt homeostasis in colorectal cancer. *Cell* 2015;161:1539–52.
43. Storm EE, Durinck S, de Sousa e Melo F, Tremayne J, Kljavin N, Tan C, et al. Targeting PTPRK-RSP03 colon tumours promotes differentiation and loss of stem-cell function. *Nature* 2016;529:97–100.
44. Han T, Schatoff EM, Murphy C, Zafra MP, Wilkinson JE, Elemento O, et al. R-Spondin chromosome rearrangements drive Wnt-dependent tumour initiation and maintenance in the intestine. *Nat Commun* 2017;8:15945.
45. Han T, Goswami S, Hu Y, Tang F, Zafra MP, Murphy C, et al. Lineage reversion drives WNT independence in intestinal cancer. *Cancer Discov* 2020;10:1590–609.
46. Sansom OJ, Meniel VS, Muncan V, Phesse TJ, Wilkins JA, Reed KR, et al. Myc deletion rescues Apc deficiency in the small intestine. *Nature* 2007;446:676–9.
47. Van der Flier LG, Sabates-Bellver J, Oving I, Haegerbarth A, De Palo M, Anti M, et al. The intestinal Wnt/TCF signature. *Gastroenterology* 2007;132:628–32.
48. Guo W, Keckesova Z, Donaher JL, Shibue T, Tischler V, Reinhardt F, et al. Slug and Sox9 cooperatively determine the mammary stem cell state. *Cell* 2012;148:1015–28.
49. Wander SA, Zhao D, Slingerland JM. p27: a barometer of signaling deregulation and potential predictor of response to targeted therapies. *Clin Cancer Res* 2011;17:12–8.
50. Gao N, White P, Kaestner KH. Establishment of intestinal identity and epithelial-mesenchymal signaling by Cdx2. *Dev Cell* 2009;16:588–99.
51. Liang X, Duronio GN, Yang Y, Bala P, Hebbar P, Spisak S, et al. An enhancer-driven stem cell-like program mediated by SOX9 blocks intestinal differentiation in colorectal cancer. *Gastroenterology* 2022;162:209–22.
52. Jennings BH, Ish-Horowicz D. The Groucho/TLE/Grg family of transcriptional co-repressors. *Genome Biol* 2008;9:205.
53. Laing AF, Lowell S, Brickman JM. Gro/TLE enables embryonic stem cell differentiation by repressing pluripotent gene expression. *Dev Biol* 2015;397:56–66.
54. Fantauzzo KA, Christiano AM. Trps1 activates a network of secreted Wnt inhibitors and transcription factors crucial to vibrissa follicle morphogenesis. *Development* 2012;139:203–14.
55. Kormish JD, Sinner D, Zorn AM. Interactions between SOX factors and Wnt/ β -catenin signaling in development and disease. *Dev Dyn* 2010;239:56–68.
56. Sancho R, Cremona CA, Behrens A. Stem cell and progenitor fate in the mammalian intestine: notch and lateral inhibition in homeostasis and disease. *EMBO Rep* 2015;16:571–81.
57. Kurppa KJ, Liu Y, To C, Zhang T, Fan M, Vajdi A, et al. Treatment-induced tumor dormancy through YAP-mediated transcriptional reprogramming of the apoptotic pathway. *Cancer Cell* 2020;37:104–22.e12.

58. Bhola PD, Letai A. Mitochondria-judges and executioners of cell death sentences. *Mol Cell* 2016;61:695–704.
59. Foronda M, Tarumoto Y, Schatoff EM, Leach BI, Diaz BJ, Zimmerman J, et al. Tankyrase inhibition sensitizes cells to CDK4 blockade. *PLoS One* 2019;14:e0226645.
60. Ianevski A, Giri AK, Aittokallio T. SynergyFinder 3.0: an interactive analysis and consensus interpretation of multi-drug synergies across multiple samples. *Nucleic Acids Res* 2022;50:W739–43.
61. Skene PJ, Henikoff JG, Henikoff S. Targeted in situ genome-wide profiling with high efficiency for low cell numbers. *Nat Protoc* 2018;13:1006–19.
62. Sato T, Stange DE, Ferrante M, Vries RGJ, van Es JH, van den Brink S, et al. Long-term expansion of epithelial organoids from human colon, adenoma, adenocarcinoma, and Barrett's epithelium. *Gastroenterology* 2011;141:1762–72.
63. Fang L, Ford-Roshon D, Russo M, O'Brien C, Xiong X, Gurjao C, et al. RNF43 G659fs is an oncogenic colorectal cancer mutation and sensitizes tumor cells to PI3K/mTOR inhibition. *Nat Commun* 2022;13:3181.
64. Lin J-R, Izar B, Wang S, Yapp C, Mei S, Shah PM, et al. Highly multiplexed immunofluorescence imaging of human tissues and tumors using t-CyCIF and conventional optical microscopes. *ELife* 2018;7:e31657.
65. Schapiro D, Sokolov A, Yapp C, Chen Y-A, Muhlich JL, Hess J, et al. MCMICRO: a scalable, modular image-processing pipeline for multiplexed tissue imaging. *Nat Methods* 2022;19:311–5.